Serotonergic modulation of visual neurons in *Drosophila melanogaster*

Maureen M Sampson[1,2]*, Katherine M Myers Gschweng[1,3]*, Ben J Hardcastle[4], Shivan L Bonanno[1,3], Tyler R Sizemore[5], Rebecca C Arnold[1,3], Fuying Gao[3], Andrew M Dacks[5], Mark A Frye[4], David E Krantz[1,3]

***These authors contributed equally**

[1]UCLA, Hatos Center for Neuropharmacology, Los Angeles, CA, USA

[2]UCLA, Molecular Toxicology Interdepartmental Program, Los Angeles, CA, USA

[3]UCLA, Psychiatry and Biobehavioral Sciences, David Geffen School of Medicine, Los Angeles, CA, USA

[4]UCLA, Department of Integrative Biology and Physiology, Los Angeles, CA, USA

[5]Department of Biology, West Virginia University, Morgantown, WV, USA

Abstract

Sensory systems rely on neuromodulators, such as serotonin, to provide flexibility for information processing in the face of a highly variable stimulus space. Serotonergic neurons broadly innervate the optic ganglia of *Drosophila melanogaster*, a widely used model for studying vision. The role for serotonergic signaling in the *Drosophila* optic lobe and the mechanisms by which serotonin regulates visual neurons remain unclear. Here we map the expression patterns of serotonin receptors in the visual system, focusing on a subset of cells with processes in the first optic ganglion, the lamina, and show that serotonin can modulate visual responses. Serotonin receptors are expressed in several types of columnar cells in the lamina including 5-HT2B in lamina monopolar cell L2, required for the initial steps of visual processing, and both 5-HT1A and 5-HT1B in T1 cells, whose function is unknown. Subcellular mapping with GFP-tagged 5-HT2B and 5-HT1A constructs indicates that these receptors localize to layer M2 of the medulla, proximal to serotonergic boutons, suggesting that the medulla is the primary site of serotonergic regulation for these neurons. Serotonin increases intracellular calcium in L2 terminals in layer M2 and alters the kinetics of visually induced calcium transients in L2 neurons following dark flashes. These effects were not observed in flies without a functional 5-HT2B, which displayed severe differences in the amplitude and kinetics of their calcium response to both dark and light flashes. While we did not detect serotonin receptor expression in L1 neurons, they also undergo serotonin-induced calcium changes, presumably via cell non-autonomous signaling pathways. We provide the first functional data showing a role for serotonergic neuromodulation of neurons required for initiating visual processing in *Drosophila* and establish a new platform for investigating the serotonergic neuromodulation of sensory networks.

Author Summary

Serotonergic neurons innervate the *Drosophila melanogaster* eye, but the function of serotonergic signaling is not known. We found that serotonin receptors are expressed in all neuropils of the optic lobe and identify specific neurons involved in visual information processing that express serotonin receptors. We then demonstrate that activation of these receptors can alter how visual information is processed. These are the first data suggesting a functional role for serotonergic signaling in *Drosophila* vision. This study contributes to the understanding of serotonin biology and modulation of sensory circuits.

Introduction

Serotonin acts a neuromodulator [1-5] in a variety of networks including the sensory systems required for olfaction, hearing, and vision [6-17]. In the mammalian visual cortex, serotonin regulates the balance of excitation and inhibition [6], cellular plasticity [18-21], and response gain [8, 22]. In some cases, the contribution of individual receptor subtypes is known; for example, in the mammalian retina, serotonergic signaling reduces GABAergic amacrine cell input to retinal ganglion cells via 5-HT1A [23] and can modulate the response to visual stimuli [24]. However, for most sensory circuits, the manner in which serotonin receptor activation is integrated to regulate information processing remains poorly understood.

The visual system of *Drosophila melanogaster* provides a powerful genetic model to study the mechanisms underlying visual circuit activity and regulation [25, 26]. In *Drosophila,* visual processing begins in the lamina where intrinsic monopolar neurons receive direct input from photoreceptors [27]. Lamina monopolar cells L1 and L2 are first-order neurons that feed into pathways discriminating light “ON” (i.e., increase in luminance) and light “OFF” (i.e.,

60 decrease in luminance) stimuli respectively [28, 29]. L1 and L2 neurons respond to changes in
61 luminance in a physiologically identical manner [30-32], while downstream neurons in the
62 medulla transform this information to discriminate ON versus OFF stimuli [29]. Further
63 processing occurs in the lobula and lobula plate to mediate higher-order computations for both
64 motion and contrast detection [29, 33, 34]. Significant progress has been made in mapping the
65 synaptic connectivity and function of visual processing neurons, including those required for
66 motion detection [27, 35-40].

67 Additional studies have shown that aminergic neuromodulators can modulate visual
68 information processing in flies and other insects [26, 41-46]. Octopamine, the invertebrate
69 equivalent of noradrenaline, is present in processes innervating the medulla and lobula in
70 *Drosophila*, where it regulates state-dependent modulation of visual interneurons [42, 46]
71 including the saliency of objects during flight [43]. Serotonergic neurons also innervate the optic
72 ganglia [47-52] and previous studies indicate that serotonin has an impact on both cellular
73 activity and visual behavior in insects [44, 45, 53, 54]. In the blowfly, serotonin alters
74 electrophysiological field recordings representing the combined output of lamina neurons [53]. In
75 the honeybee, single cell recordings in motion-sensitive lobula neurons showed that
76 serotonergic signaling reduces background activity, directional selectivity, and the amplitude of
77 field potentials evoked by moving stripes [45]. In the house fly, serotonin and other
78 neurotransmitters regulate rhythmic size changes in L1 and L2 terminals in the medulla [55] and
79 in *Drosophila*, serotonin was shown to modulate the voltage dependence of potassium channels
80 in photoreceptors [44]. Despite extensive evidence that serotonin modulates the insect visual
81 system, the molecular mechanisms responsible for these effects and the potential contributions
82 of specific subtypes of serotonin receptors remain unclear.

83 Serotonin receptor signaling occurs via diverse secondary messenger cascades [56, 57]
84 and receptors may act individually or in combination within a single cell [58, 59] or circuit [60].
85 Moreover, receptors can have different functions in different cellular compartments and can
86 induce both immediate and long-term changes in cell physiology. In addition, since serotonergic
87 modulation targets cells within larger circuits, it is likely that cell non-autonomous mechanisms
88 can induce regulatory changes in neurons that do not themselves express any serotonin
89 receptors. In sum, the precise effects of serotonin receptor activation in specific cells are difficult
90 to predict and necessitate the use of functional assays to complement expression studies.
91 Although previous studies suggest that serotonin affects visual processing, and two recent
92 studies have reported serotonin receptor expression in visual neurons [61, 62], to our knowledge
93 there is no information on the functional effect(s) of any serotonin receptor in any cell within the
94 insect visual system. In this work, we show how a specific serotonin receptor, 5-HT2B, regulates
95 visual responses in L2 lamina monopolar cells, which are critical for the initiation of visual
96 information processing. Expansion of the approach demonstrated here to other receptors and
97 cells may be used to generate a comprehensive picture of serotonergic neuromodulation within
98 a well-defined sensory circuit.

99 **Results**

100 **Distinct lamina neurons express different serotonin receptors**

101 Five genes encoding serotonin receptors have been identified in the *Drosophila* genome:
102 5-HT1A, 5-HT1B, 5-HT2A, 5-HT2B and 5-HT7 [63-67]. To identify specific optic lobe neurons
103 expressing each receptor, we expressed the marker mCD8::RFP (or GFP) under the control of
104 a recently characterized panel of T2A-GAL4 insertions in Minos-Mediated Integration Cassettes
105 (MiMICs) located in serotonin receptor gene introns [68]. The GAL4 sequence was inserted into
106 receptor-encoding genes where it acts as an artificial exon and is expected to “mimic” the
107 endogenous gene expression patterns [69]. Ribosome skipping via T2A allows GAL4 to be

expressed as a separate protein, rather than a fusion protein with the serotonin receptor [68, 70].

We observed distinct expression patterns for each receptor including projections into the optic lobe neuropils: the lamina (la), medulla (me), lobula (lo) and lobula plate (lp) (S1 Fig). We focus here on receptor subtypes showing expression in the lamina because of the ease of identifying cells based on their morphology [71] as well as the prominent role of this structure in the early stages of visual processing [28, 29, 72]. Since the primary goal of our study was to establish a role in the visual system for one or more of the receptors, it was essential that the function of some identified cells had been previously characterized.

118 To identify the specific cell types that express each serotonin receptor in the lamina, we
119 used the receptor MiMIC-T2A-GAL4 lines described above in combination with the sparse
120 labeling technique MultiColor FlpOut 1 (MCFO) [73]. Importantly, in contrast to most neurons in
121 the central brain, the stereotyped position and morphology of all neurons in the lamina as well
122 as their organization into repetitive arrays allow them to be identified on the basis of their shape
123 and location alone. Although MCFO can be used for lineage tracing [73], we induced MCFO in
124 adult flies, when visual system neurons are post-mitotic, and MCFO labeling does not represent
125 clonal events. Using 5-HT1A and 5-HT1B MiMIC-T2A-GAL4 lines with MCFO we observed a
126 subtype of cells with a soma in the medulla cortex, a long basket-like projection in the lamina,
127 and a smaller projection in the medulla (Fig 1A-B). This morphology is identical to that of T1
128 cells and distinct from other cell types in the lamina (Fig 1C) [71]. T1 cells were labeled in 23 of
129 31 brains (71%) for 5-HT1A and in 10 of 11 brains (91%) for 5-HT1B. On average, we observed
130 thirteen MCFO-labeled T1 cells per individual optic lobe for 5-HT1A and nine T1 cells per optic
131 lobe for 5-HT1B. These data are consistent with the results of recently published studies that
132 used TAPIN-Seq or FACS-SMART-Seq to analyze expression in T1 as well as other cells in the
133 visual system [61, 62] (see S2 Fig for comparison).

134 Using the 5-HT2B MiMIC-T2A-GAL4 driver with MCFO, we observed cells with a soma
135 in the lamina cortex, dense projections extending into the lamina neuropil, and a single bushy
136 terminal in the medulla (Fig 1D), a morphology identical to lamina monopolar neuron L2 and no
137 other lamina cell types (Fig 1C) [71]. We observed L2 cells in 9 of 9 (100%) 5-HT2B>MCFO
138 brains, observing an average of eleven L2 neurons per optic lobe. Additionally, we co-
139 expressed 5-HT2B>RFP with MiMIC-T2A-Lex-ChAT>GFP and found that a subset of the lamina
140 monopolar cells co-labeled with both lines, consistent with the neurochemical identity of L2 cells
141 as cholinergic (S3A Fig, arrowheads). A previous TAPIN-Seq study [61] reported a high
142 probability of 5-HT2B expression in L2 cells, consistent with these findings.

For 5-HT7>MCFO, we observed lamina monopolar cells in 7 of 13 brains (54%) (Fig 1E), with an average of 20 cells per optic lobe. Over 99% of the lamina monopolar cells labeled with 5-HT7>MCFO lacked the dense processes in the neuropil that are characteristic of L1-L3, and also lacked the vertically oriented collaterals in the inner (proximal) lamina seen in L4 neurons (Fig 1C, E). We therefore suggest that 5-HT7 is expressed in the one remaining lamina monopolar cell subtype, L5 cells, consistent with the results of another recent study [61]. Additional examples of 5-HT7>MCFO labeled L5 cells are included in S3B-C Fig.

Fig 1. Lamina neurons including T1 and L2 express serotonin receptors. (**A-E**) Serotonin receptor MiMIC-T2A-GAL4 lines were crossed to UAS-MCFO-1 to sparsely label individual cells in the lamina. Cell bodies are indicated by an arrowhead. 5-HT1A (**A**) and 5-HT1B (**B**) MCFO crosses revealed cells with morphologies identical to T1 neurons. (**C**) A diagram showing lamina neurons adapted from [71] highlights L2 (green), L5 (orange), T1 (purple), and C2 (pink). (**D**) 5-HT2B>MCFO labeled cells are morphologically identical to L2 neurons. (**E**) 5-HT7>MCFO-1 labeled neurons most likely representing L5 lamina monopolar cells. Scale bars are 20 μm and n=9-31 brains imaged per receptor subtype. Due to the nature of stochastic labeling, some cell types were observed in only a subset of brains: 22/31 (**A**), 10/11 (**B**), 9/9 (**D**), and 7/13 (**E**).

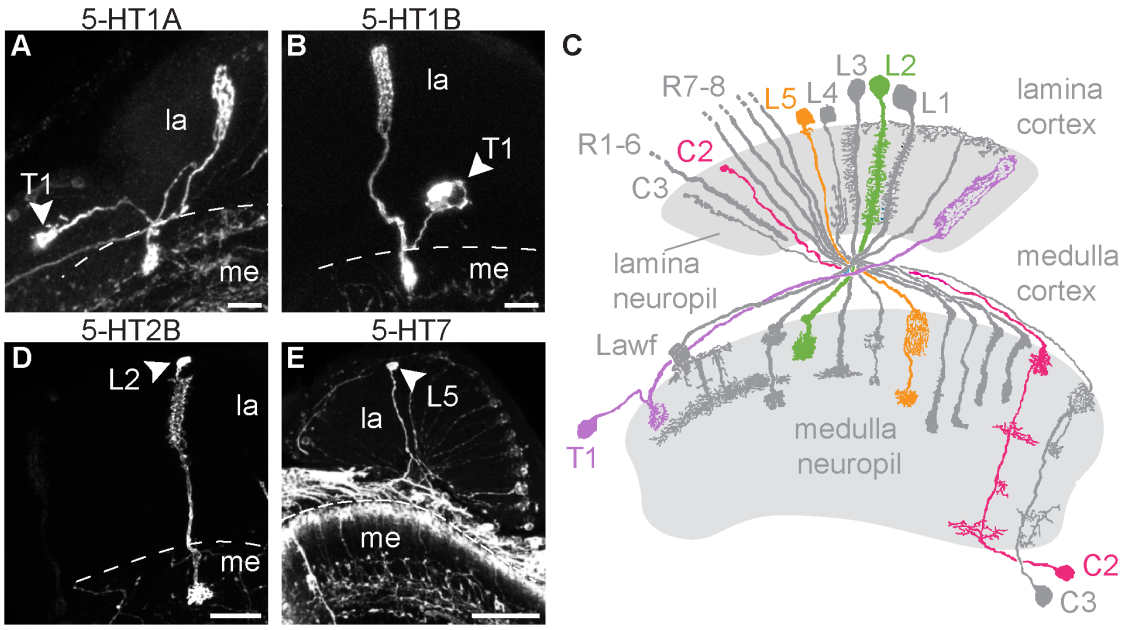

161 As noted above, multiple cells of each subtype were generally labeled in each brain.
162 However, we also detected less frequent events for other columnar cells in the lamina. These
163 include observations of multiple centrifugal C2 cells in 3 of 31 5-HT1A>MCFO brains (S3D Fig)
164 consistent with two previous reports of 5-HT1A in C2 [61, 62]. Further supporting the expression
165 of 5-HT1A in C2, we observed co-expression of 5-HT1A>RFP and MiMIC-LexA GAD1>GFP in
166 thin projections in the lamina and in cell bodies between the proximal medulla cortex and the
167 lobula plate (S2E Fig, arrowheads).

168

169 **Medulla neurons, glia and serotonergic neurons express serotonin receptors**

170 The results of other more comprehensive studies of RNA expression in visual system
171 neurons prompted us to look beyond our primary focus of lamina neurons [61, 62]. In addition to
172 the columnar neurons that express serotonin receptors and extend projections into the lamina
173 [71], we have tentatively identified cells with projections that are either confined to the medulla,
174 or include both medulla and lobula complex, and may also express serotonin receptors (S3F-H
175 Fig).

176 For 5-HT2A>MCFO, additional pleomorphic labeling was observed in the lamina cortex
177 (S4A Fig) in a pattern that appeared similar to that of optic lobe glia [74]. Anti-repo labeled nuclei
178 showed close proximity to many 5-HT2A labeled cells (S4B Fig), but one-to-one matching was
179 not possible due to irregular cell morphology. A previous microarray study of glia suggested that
180 5-HT1A and 5-HT7 are enriched in repo-GAL4 specified glia, while 5-HT1B was enriched in
181 surface glia [75]. Additionally, a previous study [61] reported expression of 5-HT7 in three types
182 of lamina glia—epithelial glia, proximal satellite glia and marginal glia.

183

184 The major ganglia of the visual system do not contain any serotonergic cell bodies;
185 rather projections from neurons in the accessory medulla and central brain innervate the optic
186 lobes. Immunolabeling for serotonergic boutons can be observed within all optic ganglia
187 neuropil as well as the lamina cortex (S5A Fig) [50, 76-79]; e.g. arborizations from 5-HT1B>GFP
188 labeled cells in the outer medulla were surrounded by a honeycomb pattern of serotonergic
189 immunolabeling (S5C Fig). Sparse labeling with 5-HT1B>MCFO co-labeled with serotonin
190 immunolabeled boutons in the inner medulla (iM), medulla layer 4 (M4), and lobula (lo) (S5E
191 Fig). Co-labeling with serotonin suggests that 5-HT1B could function as an autoreceptor in
192 these processes. A previous study also reported co-labeling between 5-HT1B-GAL4 and
193 serotonin-immunoreactive cell bodies in the subesophageal ganglion and suggested that 5-
194 HT1B may function as an autoreceptor in serotonergic neurons [80]. Another study sequenced
195 serotonergic neurons specified by TRH-GAL4 and found elevated 5-HT1A, 5-HT1B and 5-HT7
196 transcripts [81]. Although we did not comprehensively map all putative serotonin autoreceptors
197 in the central brain, we used serotonin cell maps described in [50, 76, 78, 79] to identify 5-HT1B+
198 cell clusters as LP2 (Cb1), PLP (LP1), and PMP, (S5 Fig) and 5-HT1A+ serotonergic clusters as
199 PLP (LP1), SEL, AMP and PMP (S6 Fig). The integration of functional studies in both
200 serotonergic neurons and post-synaptic neurons represents a future goal to assess the interplay
201 between auto- and post-synaptic receptors in visual circuits.

202 **L2 neurons express 5-HT2B and T1 neurons express 5-HT1A and 5HT1B**

203 Before embarking on further, time-intensive functional studies of specific neurons in the
204 lamina, we sought to confirm the expression of serotonin receptors independently of both
205 previous studies [61, 62] and the data we obtained using MiMIC-T2A-GAL4 lines. To this end,
206 we used a separate set of split-GAL4 [82] or LexA drivers previously shown to be specific for
207 particular cell types and focused on a small subset of lamina neurons: T1, L1 and L2. Drivers
208 representing each cell were used to express GFP, and the GFP-labeled cells were isolated via

209 Fluorescence Activated Cell Sorting (FACS). RNA was then extracted from T1, L1 and L2 FACS
210 isolates as well as the unlabeled cells. To probe for serotonin receptor expression in each cell
211 type, we used both RNA-Seq (Fig 2 and S1 Table) and RT-qPCR (S7 Fig and S2 Table). For
212 RNA-Seq, we compared the relative abundance for each receptor by calculating Transcripts Per
213 Million (TPMs). We found that 5-HT1A (182±43 TPM±stdev) and 5-HT1B (278±25 TPM±stdev)
214 were more abundant than other serotonin receptors (range 0.1±0.1 to 2.5±4 TPM±stdev) in T1
215 samples (N=3, Fig 2A and S1 Table). Two previous sequencing studies similarly reported the
216 expression of 5-HT1A and 5-HT1B in T1 [61, 62]. L2 isolates showed higher TPMs for 5-HT2B
217 (130±75 TPM±stdev) compared to other serotonin receptors (range 6±6 to 31±9 TPM±stdev)
218 (Fig 2B and S1 Table), also consistent with the results of another recent transcriptomic study
219 [61]. For RT-qPCR, we calculated enrichment (i.e., fold change) relative to pooled, unlabeled
220 optic lobe cells using the comparative CT method [83]. Relative to unlabeled optic lobe neurons,
221 L2 samples were enriched for 5-HT2B in 4/5 L2 samples but also showed enrichment for 5-HT7
222 and 5-HT2A in 3/5 and 5-HT2A in 1/5 samples respectively (S7 Fig and S2 Table). Although we
223 cannot rule out the presence of 5-HT2A or 5-HT7 in L2 based on the results of RT-qPCR, our
224 data and those of others [61] suggest that 5-HT2B may be the only serotonin receptor
225 abundantly expressed in L2 cells.

226 We did not observe evidence of any serotonin receptor expression in L1 neurons using
227 the serotonin receptor MiMIC-T2A-GAL4 lines to drive MCFO. In agreement with this
228 observation, RT-qPCR from isolated L1 cells (S7 Fig and S1 Table) showed virtually no receptor
229 expression, apart from one sample weakly enriched for 5-HT1B. Others have also reported a
230 low likelihood of any serotonin receptor expression in L1 neurons [61]. In sum, MCFO sparse
231 labeling in combination with RNA-Seq and RT-qPCR by our group and others [61, 62] indicate
232 that T1 neurons express 5-HT1A and 5-HT1B, and L2 neurons express 5-HT2B, whereas L1
233 neurons may not express any serotonin receptor subtypes.

234 **Fig 2. L2 neurons express 5-HT2B and T1 neurons express both 5-HT1A and 5-HT1B**
235 **serotonin receptors.** T1 or L2 neurons were isolated by FACS for RNA-Seq. Transcript
236 abundance was calculated as Transcripts Per Kilobase Million (TPMs). (**A**) T1 RNA-Seq TPMs
237 (color low to high, blue to yellow) were higher for 5-HT1A and 5-HT1B compared to other
238 serotonin receptors. (**C**) L2 RNA-Seq showed high abundance 5-HT2B in two of three samples,
239 with 5-HT2B being the most abundant serotonin receptor transcript in all replicates.

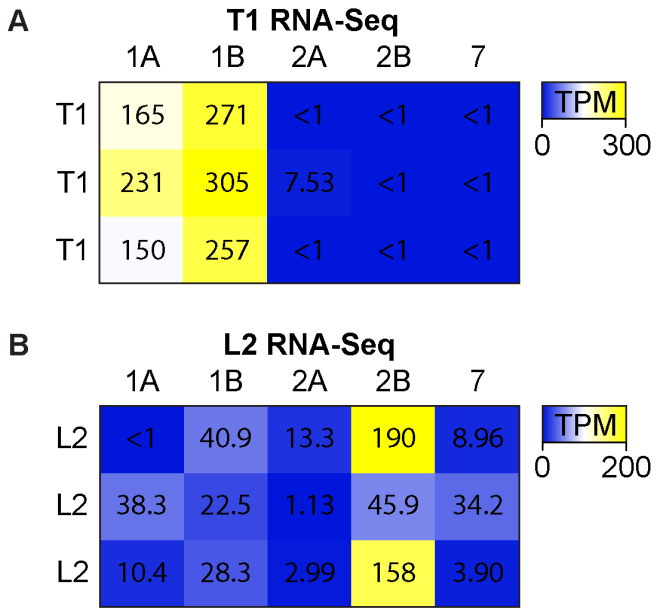

240

241

242 **5-HT2B and 5-HT1A receptors localize to the medulla neuropil**

243 Both T1 and L2 neurons have dense projections in the lamina neuropil and arborize in
244 layer 2 (M2) of the medulla neuropil. Serotonergic neurons directly innervate M1 and M2 of the
245 medulla neuropil raising the possibility that serotonergic signaling might occur at this site. If so,
246 we reasoned that the serotonin receptors expressed in L2 and T1 might localize to M1 and/or
247 M2. To test this possibility, we took advantage of a 5-HT1A allele that had been tagged at the C-
248 terminus with GFP [84]. The tag was inserted into the endogenous 5-HT1A gene, such that,
249 similar to MiMIC-T2A-GAL4 lines [68, 69], the receptor::GFP fusion protein product is putatively
250 expressed at the same level and in the same cells as the endogenous protein [84]. In
251 5-HT1A::GFP flies, we observed enrichment of the tagged protein in layer M2 of the medulla
252 relative to other subcellular sites (Fig 3A-A"), suggesting that serotonergic signaling to

253 5-HT1A::GFP expressing neurons occurs in this region. This might include T1 as well as other
254 columnar neurons that extend processes into M2. Regardless of cell type, there is very low 5-
255 HT1A::GFP signal in the lamina neuropil (Fig 3A'), suggesting that serotonergic signaling
256 primarily targets 5-HT1A receptors localized to the medulla neuropil. We also observed anti-
257 serotonin immunoreactive puncta that co-labeled with 5-HT1A::GFP in the medulla suggesting
258 that 5-HT1A could act as an autoreceptor in serotonergic projection neurons innervating the
259 medulla (Fig 3B, arrows, and S6 Fig).

260 Since we were unable to obtain an endogenously tagged allele of 5-HT2B, we relied on
261 expression of a UAS-5-HT2B::GFP transgene [85] under the control of L2-split-GAL4 to
262 investigate its subcellular localization (Fig 3C). 5-HT2B::GFP was enriched in terminals within
263 M2 of the medulla as compared to the lamina neuropil (Fig 3C-C") and showed additional
264 punctate labeling in L2 cell bodies (Fig 3C', arrowhead). To control for the possibility that all
265 membrane-bound proteins might appear to be enriched in M2, we expressed the plasma
266 membrane marker UAS-mCD8::GFP using the same L2 split-GAL4 driver. In contrast to
267 5-HT2B::GFP, labeling with mCD8::GFP was most prominent in the cell body and proximal
268 processes with progressively weaker labeling through the lamina and medulla neuropil and no
269 enrichment in layer M2 (Fig 3D"). These data strongly suggest that both 5-HT2B and 5-HT1A
270 preferentially localize to the terminals of L2 and T1 respectively in the medulla layer M2 rather
271 than the lamina neuropil. Serotonergic boutons also localize to several layers within the medulla
272 neuropil but are not found in the lamina neuropil (see S5A). It is therefore more likely that T1
273 and L2 neurons receive serotonergic signals in the medulla rather than the lamina. This may
274 occur in M2, although we cannot rule out other sites in the medulla where serotonergic boutons
275 are present, but the receptors are less enriched.

276

Fig 3. Serotonin receptors 5-HT1A and 5-HT2B are enriched in layer M2 of the medulla. (**A-A”**) 5-HT1A::GFP localized to layer M2 of the medulla, adjacent to some of the boutons in the medulla neuropil immunogenic for serotonin. Neuropil (anti-N-Cadherin, blue) and serotonin (magenta) labeling provide anatomical context for the lamina (la) and medulla (me). The region specified by the dotted lines in (**A’**) is enlarged in (**A”**). (**B-B”**) In some cases, serotonin immunoreactive boutons appear to be co-labeled rather than adjacent to 5-HT1A::GFP (arrow) possibly representing projections from serotonergic neurons in the central brain. (**C-C”**) Subcellular localization of 5-HT2B was visualized by expressing the fusion construct UAS-5-HT2B::sfGFP in L2 neurons specified by L2-split-Gal4. L2>5-HT2B::sfGFP labeling is stronger in the L2 terminals in medulla layer 2 (M2) compared to L2 projections in the lamina (la). Punctate GFP signal is observed in the L2 cell bodies (arrowhead). The region specified by the dotted lines in (**C’**) is enlarged in (**C”**). (**D-D”**) For comparison, membrane-directed UAS-mCD8::GFP was expressed in L2 neurons. L2>mCD8::GFP signal is similar in the medulla and lamina compartments. Strong GFP signal was observed in the cell bodies (arrowhead). The area within the dotted lines in (**D’**) is enlarged in (**D”**). Scale bars are 20 μm in **A-A’**, **B-B”**, **C-C’** and **D-D’**. Scale bars are 10 μm in **A”** and 8 μm in both **C”** and **D”**. Biological replicates are N=6 for 5-HT1A::GFP (**A-B**), N=15 for L2>5-HT2B::GFP (**C-C”**), and N=10 for L2>mCD8::GFP (**D-D”**).

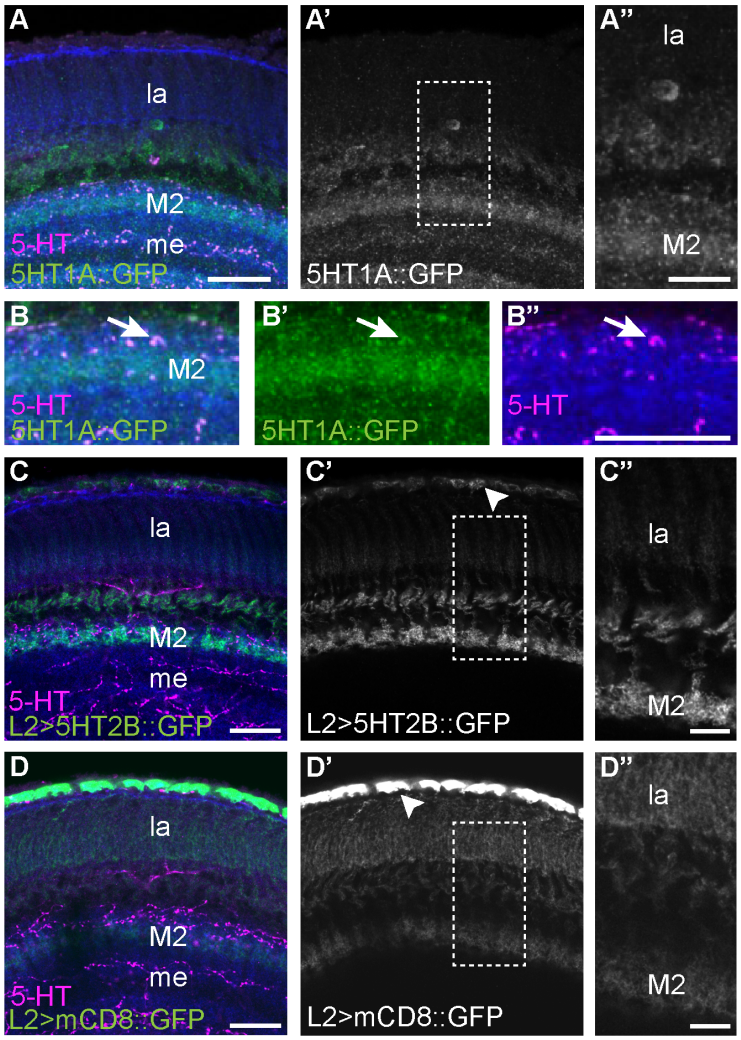

296 To further explore serotonergic signaling to L2 and T1 in the medulla, we used
297 sybGRASP to probe for potential synaptic connections between serotonergic boutons in M2 and
298 the terminals of L2 and T1 [86]. We used the previously established ultrastructural connectivity
299 of L2 onto T1 neurons in the medulla [37, 38] as a positive control to validate the use of
300 sybGRASP in detecting interactions within M2, and obtained a robust signal (S8A Fig). By
301 contrast, we failed to detect a signal in M2 in sybGRASP experiments in which the serotonergic
302 neurons were "presynaptic" to L2, T1 or L1 (S8B-E Fig). These data suggest that serotonergic
303 signaling to L2, T1 (and perhaps other columnar neurons), is more likely to be mediated by
304 volume transmission rather than true synaptic transmission, consistent with the use of volume
305 transmission by most aminergic synapses in mammalian systems [87-90].

306

307 **Serotonin increases calcium levels in L2 and L1 neurons**

308 The data presented here and by others [61, 62] strongly suggest that L2 and other cells
309 in the visual system express serotonin receptors but do not address their function. To address
310 the potential effects of serotonin on L2 neurons, we bath applied serotonin to the optic lobe and
311 used live imaging to monitor cellular activity. The data for receptor expression in L2 was
312 strongest for 5-HT2B receptors, which couple with $G_{q/11}$ to increase intracellular calcium *in vitro*
313 [67, 91]. We therefore used the genetically encoded calcium indicator GCaMP6f [92] to follow
314 changes in L2 activity that might be induced by serotonin. We again employed the L2split-GAL4
315 driver used for transcriptional analysis (Fig 2) to specifically express GCaMP6f in L2 neurons
316 (Fig 4A). Since we observed enrichment of 5-HT2B::sfGFP in L2 terminals in M2, we focused
317 our recordings of calcium signaling on these sites. For each experiment, we first recorded a
318 baseline while perfusing the tissue with saline; the perfusion solution was then switched to
319 either saline containing 100 μM serotonin or saline alone. We included tetrodotoxin (TTX) in the

320 perfusion solution in these experiments to reduce inputs to L2 neurons. TTX has been used by
321 others to study the effects of serotonin in *Drosophila,* and represents a standard method to
322 reduce cell-non autonomous neuronal inputs [93-95]

323 We consistently observed a large increase in GCaMP6f fluorescence in L2 terminals
324 following serotonin application (Fig 4B and S9A Fig). This increase continued throughout the
325 time course of the recordings, peaking at 1.73 ΔF/F ± 0.77 SEM (compared to saline control -
326 0.03 ΔF/F ± 0.05 SEM at the same timepoint; p=0.0095 by two-tailed Wilcoxon rank sum test).
327 Thus, serotonin leads to an accumulation of cytosolic calcium in L2 cells, consistent with the
328 predicted outcome of activating $G_{q/11}$ coupled 5-HT2B receptors [67, 91]. Importantly, many
329 neurons in the optic lobe use graded electrical signaling. Synaptic inputs to L2 neurons from
330 these or other cells relatively unaffected by TTX in these experiments could mediate cell non-
331 autonomous effects of serotonin in L2 neurons.

332

Fig 4. Bath application of serotonin leads to increased calcium in L2 and L1 neurons, but not T1 neurons. (**A**) The experimental setup is shown in the top of panel A, along with a sample image of L2 terminals (bottom of panel A, gray) as imaged in the medulla. (**B-D**) GCaMP6f was paired with L2, L1 and T1 split-GAL4 drivers to monitor responses to 100 μM serotonin (colored traces) or saline controls (gray traces). The perfusion change occurred approximately 105 s into the recording, which corresponds to 45 s in (B-D) because the first 60 s are not shown. (**B**) In L2 terminals serotonin application led to a significant increase in GCaMP6f signal indicating increased calcium levels as compared to saline controls (p=00095). (**C**) L1 terminals showed a similar increase in calcium following a switch to serotonin (p=0.02). (**D**) T1 cells expressing GCaMP6f showed no significant change in calcium following serotonin application (p>0.05). For (B-D) N=4-8 individual flies; the dark trace is an average of all traces and the shaded region is 1 SD; saline vs. serotonin comparisons are two-tailed Wilcoxon rank sum tests.

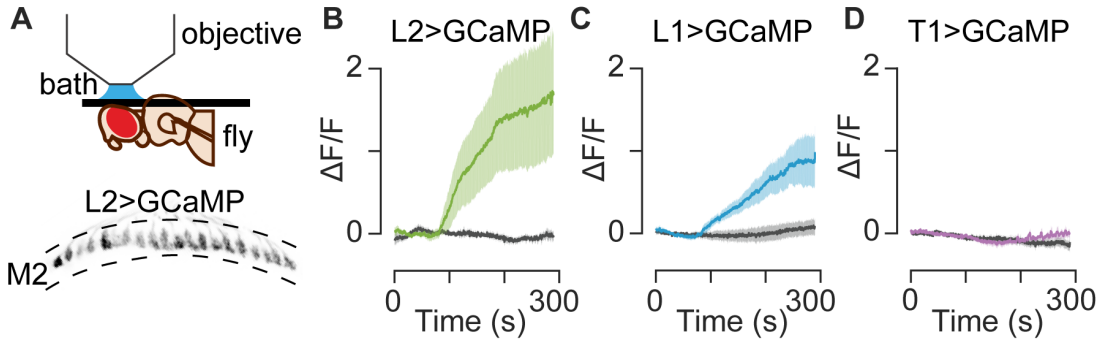

Since we did not detect serotonin receptors in L1 neurons, we did not expect serotonin to measurably change intracellular calcium levels in these cells. However, with GCaMP6f expressed in L1 cells using a cell-specific driver, we regularly observed a robust increase in baseline fluorescence following serotonin exposure (Fig 4C and S9B Fig). Although the increase in GCaMP6f signal did not reach the same response amplitude as observed in L2 neurons, the time course was similar: the signal persisted throughout the recording and peaked at 0.98 ΔF/F ± 0.34 SEM (compared to saline control at 0.07 ΔF/F ± 0.09 SEM; p=0.02 by two-tailed Wilcoxon rank sum test). A direct action of serotonin on L1 is unlikely since neither we (S7C Fig) nor others [61] detect endogenous serotonin receptors in L1 neurons. Possible mechanisms include cell-non-autonomous inputs from either columnar or non-columnar neurons intrinsic to

358 the visual system, more distal projections from the central brain or perhaps electrical coupling
359 between L1 and L2 [28]. The cell non-autonomous inputs mediating the indirect effects of
360 serotonin would seem be more likely to use graded potentials, as is common in the visual
361 system [96-98], since TTX was included in the perfusion solution in these experiments and TTX
362 blocks sodium channels that are required for action potentials [94, 95]. However, we cannot rule
363 out the possibility that TTX blocked channels mediating additional modes of communication.

364 We next examined whether serotonin could affect the activity of T1 cells. Both 5-HT1A
365 and 5-HT1B receptors, expressed in T1 neurons, are expected to couple with G_i proteins and
366 negatively regulate adenylyl cyclase [65, 91]. Due to the generally inhibitory function of these
367 receptors, we hypothesized that serotonin would dampen activity in T1 neurons, possibly
368 manifested as a decrease in cytosolic calcium or membrane potential [99]. Using the T1 split-
369 GAL4 driver [82] to express either GCaMP6f or the voltage sensor Arclight [100], we did not
370 observe a significant change in fluorescence during perfusion with serotonin (Fig 4D, S9C-D
371 Fig) $p>0.1$). Thus, further experiments will be needed to determine the effects of serotonin on
372 T1 neurons. These negative data are nonetheless important for the current study, since the
373 absence of a GCaMP6f response in T1 neurons indicates that the responses observed in L1
374 and L2 are not artifacts or a generalized phenomenon common to all cells in the lamina.

375

376 **Serotonin in visual processing**

377 To explore the possibility that serotonergic neuromodulation plays a role in visual
378 processing, we tested whether exogenous serotonin alters visually induced calcium transients in
379 L2 neurons. We used GCaMP6f to record and compare calcium transients in flies receiving
380 saline or serotonin perfusion. Previous studies using voltage indicators found that L2 neurons
381 depolarize in response to dark flashes and hyperpolarize in response to light flashes [31].

382 Similarly, calcium-indicator recordings showed that intracellular calcium increased in the dark
383 and decreased in the light in [30]. Brief light or dark flashes induce bi-phasic calcium transients
384 [31] that enable analysis of calcium kinetics. For this reason, we used brief dark or light flashes
385 to test whether serotonin might alter the magnitude or kinetics of visually induced calcium
386 transients in L2 terminals. Flies were suspended over an LED arena (see Fig 4A) and either a
387 light or dark flash of the entire LED screen (100 ms) was presented at 5 s intervals. Between
388 each flash, the screen showed an intermediate brightness level, indicated as grey in Fig 5A.
389 One-minute "epochs" consisting of 12 flashes of randomly shuffled polarity were presented six
390 times for each trial (Fig 5A). The first 60 s epoch was recorded in saline alone, followed by a
391 switch to either saline with 100 μM serotonin or saline alone during epoch 2 (Fig 5A). Unlike the
392 experiments shown in Fig 4, we did not include TTX in the perfusion solutions because we did
393 not want to affect neuronal communication in any way that might interfere with the response to
394 visual stimuli. Performing additional further experiments in the absence of TTX was also
395 important to rule out the possibility TTX was responsible for the effects seen in Fig 4.

396 Dark flashes induced a large increase in calcium that returned to baseline within ~1
397 second as previously described [31] (Fig 5B). The amplitude of the dark flash induced calcium
398 transients increased over the time course of the experiment for animals receiving either
399 serotonin or saline (Fig 5B). To compare differences between the serotonin and saline control
400 groups and the potential effects of serotonin over the time course of the experiment, we
401 quantified three calcium transient variables: amplitude (5C), the time required for decay from the
402 peak to a subsequent minimum (5C'), and the slope of the decay (5C''). To facilitate the direct
403 comparison of results obtained during perfusion with saline alone versus saline followed by
404 serotonin, we first calculated the average for each variable prior to serotonin exposure
405 measured during epoch-1. We then subtracted the epoch 1 baseline from each epoch,
406 effectively setting the initial value of each plot to 0 for epoch 1 in Fig 5C-C".

407 Fig 5C shows the change in calcium transient amplitude, calculated as the difference
408 between the pre-stimulus ΔF/F and the peak ΔF/F, relative to epoch 1. We did not detect a
409 difference between the serotonin and saline groups. Fig 5C' quantifies the decay time from peak
410 amplitude, calculated as the time (s) between the peak ΔF/F and the subsequent minimum
411 ΔF/F, relative to epoch 1. We detected a modest but statistically significant (p=0.0036 by
412 Repeated Measures ANOVA) increase in the decay time of the dark flash response in animals
413 perfused with serotonin versus saline alone. In Fig 5C" we quantify the change in the slope of
414 the decay relative to epoch 1; we did not detect a difference in slope between flies treated with
415 serotonin versus saline (Fig 5C").

416 Light flashes induced a transient decrease in GCaMP6f fluorescence, followed by a
417 secondary sustained rebound (Fig 5D) as previously reported [31]. To analyze calcium
418 transients induced by light flashes, we quantified three variables: the magnitude of the initial
419 calcium decrease relative to the pre-stimulus baseline (Fig 5E), the time from minimal to
420 maximal ΔF/F (Fig 5E'), and the slope of this rebound (Fig 5E''). Baseline values obtained for
421 the response to light flashes in epoch 1 were subtracted from each epoch to set the initial value
422 of each variable to 0 for epoch 1 in the plots in Fig 5E-E". We did not observe any significant
423 differences between saline and serotonin groups when calculating the magnitude of the initial
424 downward deflection (Fig 5E), the time from minimal to maximal ΔF/F (Fig 5') or the slope of the
425 rebound (Fig 5E").

426 In sum, serotonin drove a robust increase in intracellular calcium levels of L2 neurons in
427 wildtype flies, regardless of the presence (Fig 4) or absence (Fig 5) of TTX. We also detected a
428 modest, but statistically significant effect of serotonin on the kinetics, but not the amplitude, of
429 the GCaMP6f response of L2 to a dark flash (Fig 5C'). We did not detect any effect of serotonin
430 on the response of L2 to a light flash in 5-HT2B +/+ flies.

431

432 **Fig 5. Serotonin modulates L2 neuron visually induced calcium transient kinetics**. L2-
433 split-GAL4 was crossed to UAS-GCaMP6f to monitor calcium transients following 100-ms light
434 or dark flashes. The optic lobe was initially perfused with saline alone during a 60 s baseline
435 recording designated as "epoch 1". The solution was then switched to either saline with
436 serotonin or saline control after 105 s, with the switch occurring during epoch 2. (**A**) A sample
437 recording with serotonin perfusion following the initial baseline is shown in the upper panel.
438 Light or dark stimuli (A, middle panel) were flashed at random every 5 s for 6 min. To visualize
439 changes in the response to light and dark flashes in L2, data from each 60 s epoch was binned
440 (see epochs 1-6 in A, lower panel). (**B**) Response to dark flashes. Color coded traces
441 representing each 60 s epoch are shown for flies receiving saline (left panel, cyan to blue) or
442 serotonin perfusion (right panel, yellow to red). In both groups, L2 terminals responded to a dark
443 flash with a strong increase in GCaMP6f fluorescence before returning to baseline. (**C-C"**)
444 Analysis of dark flash response from panel B. For plotting each variable shown in C, the
445 average value for the epoch 1 baseline was subtracted; epoch 1 is therefore always set to 0 in
446 panel C-C". (**C**) The change in the amplitude of the calcium transient (the difference between
447 pre-stimulus ΔF/F and maximum ΔF/F) relative to epoch 1 is shown in (C) and did not differ
448 between flies exposed to saline versus serotonin. (**C'**) The change in the time (s) to reach a
449 minimum ΔF/F following the maximum ΔF/F relative to epoch 1 is shown in (C') and was
450 significantly longer ($p \leq 0.01$**) in serotonin-perfused flies compared to saline controls. (**C"**) The
451 change in the slope of the decay from maximum ΔF/F to minimum ΔF/F relative to epoch 1 was
452 not different between the saline and serotonin groups. (**D**) Response to light flashes. When a
453 light flash was presented in control experiments, L2 cells responded with a decrease in GCaMP
454 signal followed by a large sustained rebound. Color coded traces representing each 60 s epoch
455 for saline (left panel, cyan to blue) and serotonin (right panel, yellow to red) are shown. (**E-E"**)
456 Analysis of light flash response from panel D. For plotting each variable shown in E, the average
457 value for the epoch 1 baseline was subtracted; epoch 1 is therefore always set to 0 in panel E-
458 E" as in panel C-C". (**E**) The change in the amplitude of the initial decrease in calcium (the
459 difference between pre-stimulus ΔF/F and the subsequent minimum ΔF/F) relative to epoch 1 is
460 shown in (E) and was not different between the saline and serotonin groups. (**E'**) The change in
461 the time to reach a maximum ΔF/F (time, s) relative to epoch 1 and (**E"**) the change in the slope
462 of the rebound relative to epoch 1 was not significantly differ between serotonin versus saline
463 controls. Recordings in B-E represent, N=14 and N=20 individual flies perfused with serotonin or
464 saline respectively. Shaded areas show mean +/- SEM. Comparisons are two-way repeated
465 measures ANOVA (brackets show interactions between time and genotype) and Sidak's
466 multiple comparisons tests, $p \leq 0.05$ *, $p \leq 0.01$**, $p \leq 0.001$***, $p \leq 0.0001$****.

467

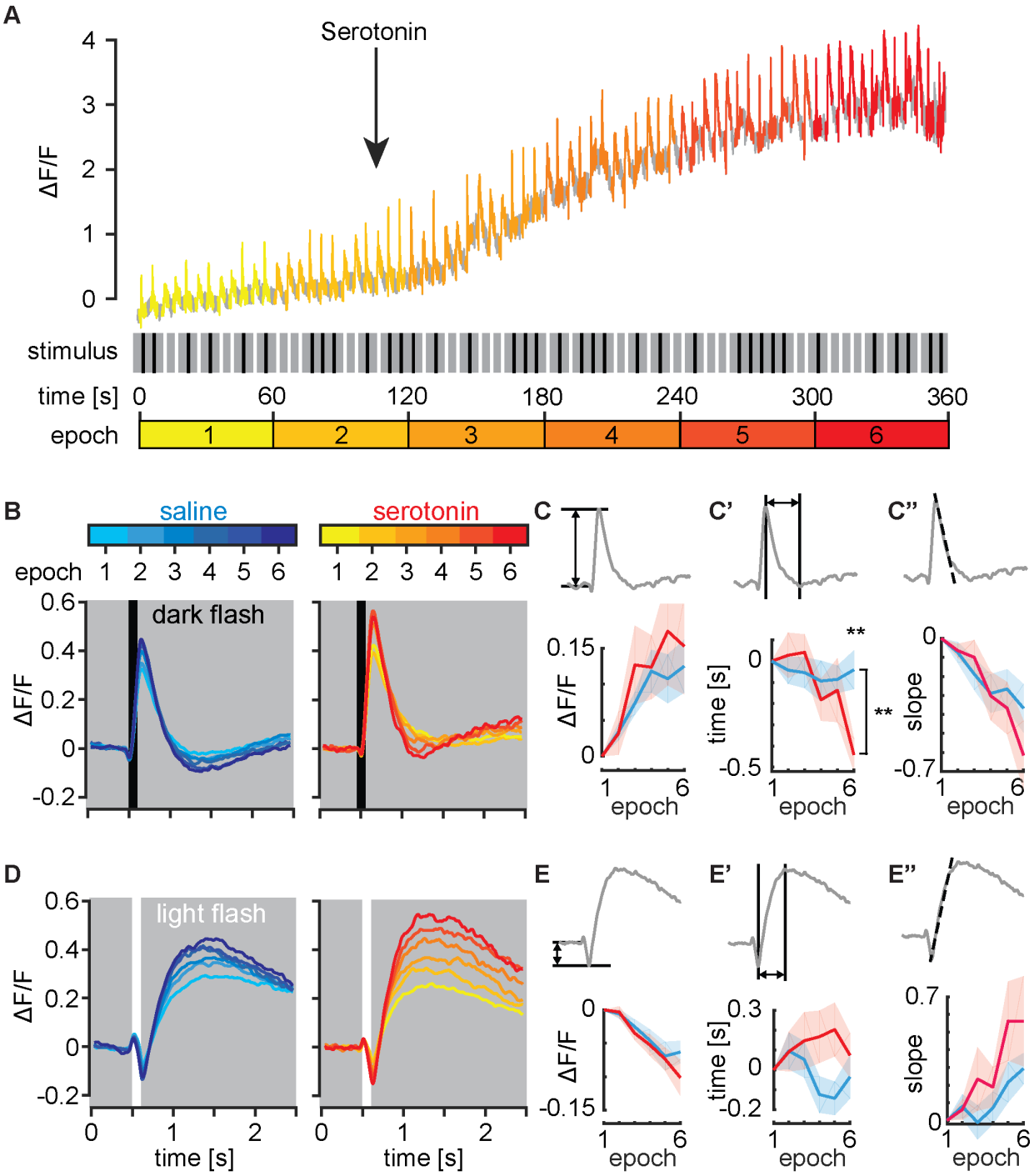

468

469

470

471

472 **5-HT2B mediates the effects of serotonin on L2**

473 Since 5-HT2B is expressed in L2 neurons and is predicted to use calcium as a second
474 messenger we hypothesized that it would mediate the response of L2 neurons to serotonin. In
475 flies expressing wild type 5-HT2B we observed a robust serotonin-mediated increase in
476 intracellular calcium (Fig 4B, with TTX in the perfusion solution and Fig 6A, without TTX in the
477 perfusion solution). We next examined whether loss of 5-HT2B would blunt the gradual increase
478 in baseline calcium we observed in flies exposed to serotonin (Fig 6B). As a negative control for
479 experiments using the 5-HT2B homozygous mutants (-/-) we used heterozygous siblings (+/-) in
480 which one wild type allele of 5-HT2B was present (Fig 6B). Similar to 5-HT2B +/+ flies (Fig 6A),
481 5-HT2B heterozygous controls perfused with serotonin showed a gradual increase in baseline
482 calcium levels over the six-minute time course of the experiment (Fig 6B). In contrast, in the
483 5-HT2B -/- mutant, the baseline calcium signal was nearly flat over the time course of the
484 experiment ($p=0.0024$ by two-tailed Wilcoxon rank sum test). To more specifically reduce the
485 expression of 5-HT2B in L2, we also tested available RNAi transgenes directed against 5-HT2B
486 but did not detect a significant effect (data not shown). We therefore cannot rule out indirect cell
487 non-autonomous effects from 5-HT2B expression in other cell types. However, the simplest
488 explanation for the observed results is that activation of 5-HT2B in L2 neurons generates a
489 gradual increase in cytosolic calcium.

490 We next examined whether loss of 5-HT2B would alter the calcium transients in L2
491 neuron terminals following light or dark flashes. We hypothesized that loss of 5-HT2B would
492 block any changes in the kinetics of the calcium response seen with serotonin perfusion (see
493 Fig 5C'). We also reasoned that a mutation in the serotonergic signaling pathway might provide
494 a "sensitized genetic background" to enhance the detection of serotonin's functional effects. As
495 a negative control, we used heterozygous siblings (5-HT2B +/-). We again graphed averages for
496 each epoch after subtraction of the average for epoch-1. For dark flashes, we plotted the
497 change in amplitude of the increase from pre-stimulus $\Delta F/F$ to the maximum $\Delta F/F$ relative to

498 epoch 1 (Fig 6D), the change in the time between the peak ΔF/F and the subsequent minimum
499 ΔF/F relative to epoch 1 (Fig 6D'), and the change in slope of the decay relative to epoch 1 (Fig
500 6D"). As we observed in 5-HT2B +/+ flies (see Fig 5C'), perfusion of 5-HT2B +/- heterozygous
501 controls with serotonin led to a gradual reduction in the time required for L2 terminals to reach a
502 minimum after responding to a dark flash (Fig 6D'). In striking contrast, in 5-HT2B -/-
503 homozygous loss of function flies, the time between the peak and the subsequent minimum (Fig
504 6D'), and the slope of the decay (Fig 6D") remained unchanged over the course of the
505 experiment and continuous perfusion with serotonin. In sum, the 5-HT2B mutation ablated the
506 serotonin-dependent change in the kinetics of the L2 response to dark flashes. The effects on
507 amplitude (Fig 6D) were not statistically significant between the 5-HT2B -/- mutant and
508 heterozygous controls.

509 To compare how 5-HT2B +/- and 5-HT2B -/- flies responded to light flashes, we
510 calculated the change in the amplitude of the initial downward deflection from the pre-stimulus
511 baseline relative to epoch 1 (Fig 6F), the change in the time from minimal to maximal ΔF/F
512 relative to epoch 1 (Fig 6F') and the change in the slope of the rebound relative to epoch 1 (Fig
513 6F"). The 5-HT2B +/- heterozygotes preparations showed a progressive increase in the
514 magnitude of the initial downward deflection (Fig 6F); strikingly, this progression was absent in
515 5-HT2B -/- mutants and the difference between the time course of the heterozygotes and
516 homozygotes was highly significant ($p \leq 0.0001$) (Fig 6F). Similarly, the change in both the time
517 required for ΔF/F to progress from a post-stimulus minimum to secondary maximum (Fig 6F')
518 and the slope of the rebound relative to epoch 1 were significantly different (Fig 6F"). Together,
519 the differences between 5HT2B +/- and 5-HT2B -/- in the response to a dark flash (Fig 6D-D")
520 and these data strongly suggest that 5-HT2B mediates the effects of serotonin on the response
521 of L2 neurons to at least one type of visual stimulus, although we cannot yet conclude whether
522 this occurred in a cell-autonomous manner.

Fig 6. 5-HT2B mediates the L2 neuron response to serotonin. (**A**) L2-split-GAL4>GCaMP6f was used to monitor intracellular calcium in L2 terminals. The optic lobe was initially perfused with saline alone and was then switched to either saline with serotonin or saline control after 105 s. Serotonin perfusion (in the absence of TTX) induced an increase in baseline calcium in 5-HT2B +/+ lines receiving serotonin compared to saline controls. (**B**) Mutant 5-HT2B-"KO"-GAL4 flies (5-HT2B -/-) were combined with UAS-GCaMP6f to monitor calcium changes in L2 terminals. Homozygous (5-HT2B -/-) and heterozygous (5-HT2B +/-) flies both received serotonin perfusion. The serotonin-mediated baseline increase was seen in 5-HT2B +/- flies, as in wild type flies, but was not observed in 5-HT2B -/- flies. (**C-F**) Homozygous (5-HT2B -/-) and heterozygous (5-HT2B +/-) 5-HT2B- "KO" -GAL4 flies expressing UAS-GCaMP6f were used to record calcium transients following brief light or dark flashes. The preparation was initially perfused with saline alone during a 60 s baseline recording designated as epoch 1 and the solution was then switched to saline with serotonin after 105 s, with the switch occurring in epoch 2. (**C**) Response to dark flashes. Traces representing each 60 s epoch (yellow to red) are shown for 5-HT2B +/- (left) and 5-HT2B -/- (right). All preparations received serotonin perfusion. In both groups, dark flashes induced a strong, transient increase in GCaMP6f fluorescence that returned to baseline. Dark-flash calcium transient amplitude increased over the course of the experiment for 5-HT2B +/- flies, but this was not seen in 5-HT2B -/- flies. (**D-D"**) Analysis of dark-flash data from panel C. For plotting each variable shown in D-D", the average value for epoch 1 was subtracted; epoch 1 is therefore always set to 0. (**D**) The change in the amplitude of the maximum calcium transient (the difference between pre-stimulus ΔF/F and maximum ΔF/F) relative to epoch 1 is shown. (**D'**) The change in the time to reach a minimum ΔF/F following the maximum ΔF/F of the calcium transient relative to epoch 1 was significantly decreased in 5-HT2B +/- flies compared to 5-HT2B -/- flies in which this period was essentially unchanged over the time course of the experiment. (**D"**) The change in the slope of the decay relative to epoch 1 was significantly decreased in 5-HT2B +/- flies compared to 5-HT2B -/- flies; it appeared essentially unchanged for 5-HT2B -/- flies over the course of the experiment. (**E**) Response to light flashes. When a light flash was presented, L2 cells responded with a decrease in the GCaMP6f signal followed by a large sustained rebound. Responses for 5-HT2B +/- (left) and 5-HT2B -/- (right) flies are shown. (**F-F"**) Analysis of light flash data from panel E. For plotting each variable shown in F-F", the average value for the epoch 1 baseline was subtracted; epoch 1 is therefore always set to 0 as in panels D-D". (**F**) The change in the amplitude of the light flash induced a calcium decrease (calculated as the difference between the pre-stimulus ΔF/F and minimum ΔF/F) relative to epoch 1 that was significantly enhanced over the course of the experiment in 5-HT2B +/- flies relative to 5-HT2B -/- flies. (**F'**) The change in the time to reach a maximum relative to epoch 1 was significantly decreased in 5-HT2B -/- flies compared to the response of 5-HT2B +/- flies which appeared unchanged. (**F"**) The change in the rebound slope relative to epoch 1 increased significantly in 5-HT2B +/- flies relative to 5-HT2B -/- flies. For (A), N=14 serotonin and N=20 saline exposed flies were tested. For (B-F), N=13 5-HT2B +/- and N=15 5-HT2B -/- flies, all receiving serotonin, were tested. Shaded areas show mean +/- SEM. Comparisons in (D, F) are two-way repeated measures ANOVA (brackets show interactions between time and genotype) and Sidak's multiple comparisons tests, $p \leq 0.05$ *, $p \leq 0.01$**, $p \leq 0.001$***, $p \leq 0.0001$****.

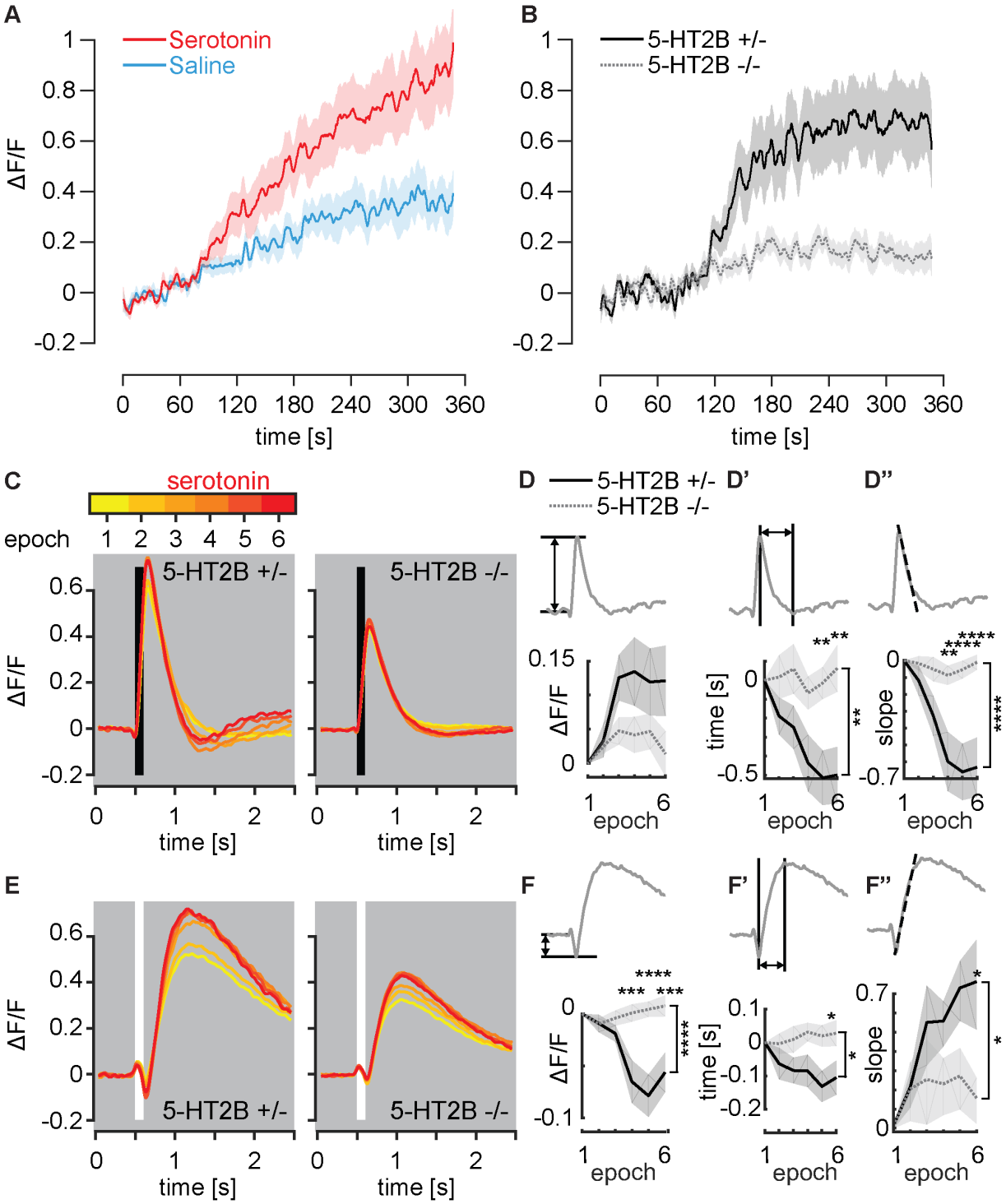
A
Serotonin
Saline
ΔF/F
time [s]
B
5-HT2B +/-
5-HT2B -/-
time [s]
C
serotonin
epoch
5-HT2B +/-
5-HT2B -/-
ΔF/F
time [s]
D
5-HT2B +/-
5-HT2B -/-
D'
D''
ΔF/F
time [s]
slope
epoch
E
5-HT2B +/-
5-HT2B -/-
ΔF/F
time [s]
F
F'
F''
ΔF/F
time [s]
slope
epoch

569 **Discussion**

570 Serotonergic modulation occurs by activation of multiple receptors and associated
571 secondary messenger cascades [56, 57]. Understanding how serotonergic signaling tunes
572 circuit activity requires functional experiments to determine the effects on specific cells in
573 addition to mapping the cellular and subcellular cites of individual receptors. Previous studies
574 have mapped the expression pattern of multiple receptor subtypes to specific cells within the
575 visual system [61, 62]. To develop the fly visual system as a new molecular-genetic model to
576 study serotonergic neuromodulation we have confirmed the expression of the five *Drosophila*
577 serotonin receptors in a subset of experimentally tractable cells in the lamina and used live
578 imaging to determine their potential function. To our knowledge, these represent the first
579 functional data for serotonergic neuromodulation of the *Drosophila* visual system with the
580 exception of a single report in 1995 [44]. We also present the first data on the subcellular
581 localization of serotonin receptors in the visual system. In addition, our data mapping the cellular
582 expression pattern of the receptors are complementary to two previous transcriptomic analyses
583 [61, 62] since we have used a different experimental approach.

584 We focused primarily on the lamina to identify a subset of cells that might express
585 serotonin receptors. Our goal was to identify cells that could be used for further functional
586 studies and the function of several lamina neurons have been previously characterized [29, 34,
587 82, 101]. In addition, the lamina contains a relatively small number of neurons, allowing
588 identification based on morphology alone [71]. MiMIC-T2A-GAL4 drivers [68] are useful for
589 replicating the endogenous expression patterns and provided a convenient method to screen for
590 cells that express each receptor (Fig 1, S1, S3-6). To validate receptor expression before
591 performing functional studies we used a combination of MiMIC-based reporter lines, RNA-Seq
592 and RTq-PCR. All of these techniques indicated that 5-HT2B is expressed in L2 lamina
593 monopolar neurons, which are involved in motion [28, 102] and contrast vision [34]. The idea that

594 L2 cells express 5-HT2B is further supported by data from a previous report that mapped
595 neurotransmitter receptor transcripts to cells throughout the visual system [61]. Although our RT-
596 qPCR supports the possibility that L2 neurons might also express 5-HT7, neither we nor others
597 detect an enrichment of 5-HT7 using RNA-Seq [61].

598 We observed consistent expression of 5-HT1A and 5-HT1B in T1 neurons, whose
599 function remains poorly understood [82]. We did not detect expression of any serotonin
600 receptors in the L1 subclass of lamina monopolar neurons, which acts in parallel to L2 for visual
601 processing. Our data on T1 and L1 are consistent with recent transcriptional studies of these
602 and other cells in the visual system [61, 62]. Konstantinides et al. used FACS-SMART-Seq
603 (GSE103772) and found 5-HT1A and 5-HT1B in T1 cells, 5-HT7 in Mi1 cells, and 5-HT1A in C2
604 cells. Davis et al. used TAPIN-seq [61] and also reported 5-HT2B in L2 cells, 5-HT1A in C2
605 cells, and 5-HT7 in L5 cells, consistent with the sparse labeling experiments shown here in Fig 1
606 and S3. In S2 Fig we directly compare serotonin receptor expression reported for each cell type
607 in the current study, Davis et al. [61], and Konstantinides et al. [62].

608 Differences in the methods used to isolate target cell populations, extract RNA, and
609 create DNA libraries can impact sequencing results. For example, Davis et al. used TAPIN-seq
610 to purify nuclei, subjecting tissue homogenates to two rounds of immunoprecipitation to isolate
611 tagged nuclei before preparing RNA, a process which may lead to non-specific binding.
612 Conversely, our use of FACS can lead to contamination by other cell types due to incomplete
613 dissociation of GFP-tagged cells or due to non-specific labeling by the driver lines. Additionally,
614 differences in cDNA library construction, including different approaches for poly-A mRNA
615 enrichment, can significantly affect the results obtained in different studies. In contrast to Davis
616 et al. we did not detect expression of serotonin receptors in photoreceptor cells or in lamina
617 monopolar neuron L3 using MiMIC-T2A-GAL4>UAS-MCFO. These inconsistencies could be
618 due to biological variability in levels of gene expression or infidelity in the MiMIC-based

619 approach, which may not perfectly reflect endogenous expression due to disruption of the
620 genetic locus. Further studies may reconcile these differences; meanwhile we suggest that
621 using multiple, overlapping methods may be important to fully evaluate complex patterns of
622 gene expression.

623 Our results suggest serotonin receptor expression in lamina glia (S4 Fig). Possible roles
624 for glia in the visual system have been suggested previously and studies of RNA expression in
625 glia suggest a possible enrichment in some subtypes of serotonin receptors [103, 104]. The
626 presence of serotonin receptors in glia immediately adjacent to the basement membrane of the
627 retina raises the possibility that they could regulate photoreceptor cells in a non cell-
628 autonomous manner. The only prior report on acute serotonergic signaling events in the
629 *Drosophila* visual system described the modulation of potassium channels in photoreceptors
630 [44]. However, the ex vivo preparations used for these experiments may have included other
631 cells or cell fragments, and unlike a previous transcriptomic study [61], we did not detect
632 serotonin receptor expression in photoreceptors. We therefore speculate that serotonin could
633 regulate photoreceptors non-autonomously as we report for L1 either via inputs from other
634 neurons or perhaps glia [27, 44, 105].

635 Serotonergic signaling occurs via G-protein coupled receptors, which can induce
636 immediate or long-term changes in cell physiology. We examined acute responses to serotonin
637 receptor activation by bath applying serotonin onto optic lobe tissue. Consistent with the
638 predicted coupling of 5-HT2B to G_q, we found that L2 neurons respond with a robust increase in
639 calcium measured by GCaMP6f fluorescence (Fig 4B, Fig 6A, S9A Fig) and this effect was
640 dramatically reduced in 5-HT2B -/- flies (Fig 6B). The simplest explanation for these effects is
641 that 5-HT2B regulates L2 in a cell autonomous manner. However, it remains possible that
642 5-HT2B expressed in other cells could contribute to the effects we observe. Specific knockdown
643 of 5-HT2B in L2 neurons will be required to address this important issue, but available 5-HT2B

644 RNAi lines have been ineffective in our hands, and additional genetic tools will be needed to
645 perform cell type specific knock down or knock out experiments [106]. Additional experiments
646 will also be needed to assess the potential developmental effects of the 5-HT2B mutant. Finally,
647 we cannot completely rule out the possibility that 5-HT7 could contribute to the regulation of at
648 least some L2 cells (see S7B Fig). These limitations aside, our data indicate that 5-HT2B plays
649 a role in regulating one of the cells required for most visual processing in the fly.

650 In L1 neurons, which do not express serotonin receptors, we unexpectedly observed a
651 large calcium response to serotonin similar to that of L2 neurons (Fig 4C). These data suggest
652 that L1 cells are indirectly regulated by input from other cells, but further studies will be needed
653 to determine the underlying mechanism. The most likely explanation would seem to be indirect,
654 non-autonomous activation of L1 neurons by input from cells that express serotonin receptors
655 either in the optic lobes or perhaps the central brain. Either synaptic or non-synaptic inputs from
656 neighboring columnar neurons or from wide field neurons that innervate multiple layers of the
657 medulla or glia could be responsible for these effects. TTX was included in solutions used for
658 the experiments on L1 shown in Fig 4. TTX blocks sodium channel-based action potentials and
659 graded potentials, which have been well documented in the insect brain including photoreceptor
660 cells and other optic lobe neurons, and could contribute to non-autonomous regulatory effects in
661 the presence of TTX; however, we cannot rule out the possibility that TTX affects sodium
662 channels expressed by cells that use graded potentials [96-98]. We also note that GABAergic
663 C2 neurons [107] express 5-HT1A (S2 Fig, S3D-E Fig) and are known to synapse onto L1 in M1
664 [36]. Likewise, L5 neurons express the 5-HT7 receptor (Fig 1E, S2 Fig) and reciprocally synapse
665 with L1 neurons in M1 and M5 [36]. Alternatively, it is possible that the gap junctions that couple
666 L1 and L2 neurons or interactions with glia could mediate indirect serotonergic regulation of L1
667 [28]. Regardless of the underlying mechanism, our data highlight the importance of indirect
668 pathways for the serotonergic modulation of circuit activity.

669 Multiple neuroanatomical experiments, including data presented here (S5 Fig), show that
670 serotonergic boutons are distributed within several layers of the medulla neuropil including M1,
671 M2, M4 and the inner medulla (iM) [50, 78, 108, 109]. By contrast, they are absent from the
672 lamina neuropil. We found that a molecularly tagged version of 5-HT2B expressed in L2
673 neurons was enriched in the medulla neuropil, most prominently in layer M2 (Fig 3). A tagged
674 version of 5-HT1A expressed via the 5-HT1A locus in T1 and other cells localized to a similar
675 site in the medulla neuropil (Fig 3). These data strongly suggest that the medulla rather than the
676 lamina is the most relevant site for serotonergic regulation of these cells. The lamina cortex,
677 which contains the somata of L2 and other monopolar cells is also innervated by serotonergic
678 processes; however, to our knowledge there is no data in flies in support of the aminergic
679 innervation of cell bodies rather than the neuropil.

680 Similar to most other circuits, serotonergic signaling to L2 in the medulla is likely to occur
681 extrasynaptically. In both mammals and insects, serotonin can be released extra-synaptically
682 through volume transmission [88, 110] or through synaptic sites [48, 111-114]. However, the
683 majority of mammalian aminergic release sites lack an identifiable synaptic partner, and even
684 synaptic release can lead to spillover and extrasynaptic release. Ultrastructural studies in the fly
685 visual system have established a connectome for many neurons in the lamina and medulla
686 including L1, L2 and T1 neurons. By contrast, the ultrastructure of serotonergic and other
687 aminergic processes in the optic lobe of *Drosophila* are not known. Serotonergic release sites
688 appear to lack synaptic partners in the lamina of the blowfly *Calliphora* [115] and our data using
689 sybGRASP to test whether serotonergic neurons synapse on L2, T1, and L1 was negative (S8
690 Fig). It is possible that ultrastructural studies will prove more fruitful, but in the absence of true
691 synaptic connections we anticipate that new methods may be needed to unambiguously
692 determine the relationship of aminergic boutons to potential targets in the visual system.

693 In T1 neurons, we were unable to detect any acute changes in baseline calcium or
694 voltage in response to serotonin application (Fig 4D and S9C-D Fig) and other probes (e.g., for
695 cAMP) may be necessary to detect the acute response of T1 to serotonin. However, it is also
696 possible that activation of 5-HT1 receptors does not induce any acute physiological response,
697 and that more chronic indices will necessary to detect the potential effects of serotonin on T1
698 neurons. For now, the absence of a GCaMP6f response in T1 neurons serves as an important
699 negative control and demonstrates the specificity of the responses observed in L1 and L2.

700 In *Drosophila*, L1 and L2 neurons detect changes in luminance and together are
701 necessary for the full complement of motion vision. Both neurons receive synaptic input from
702 photoreceptors, and respond to luminance changes with graded potentials, depolarizing in dark
703 conditions and hyperpolarizing in light [30-32]. These two neurons feed forward into parallel
704 pathways to enable further visual processing such as motion and contrast detection [29, 34,
705 101]. The modulation of visually induced calcium transients in L2 following serotonin application
706 (Fig 5-6) suggests a role for serotonin in potentiating the response of L2-dependent visual
707 processing pathways [31]. Our data also suggest a molecular-mechanism for previous
708 observations made in larger insects including serotonin-induced changes field recordings in
709 blowfly representing the output of lamina monopolar cells [53] and honeybee motion detection
710 in the lobula [45].

711 The effects of serotonin on calcium signaling in L2 cells were readily apparent in
712 experiments comparing its effects on 5-HT2B homozygous mutants versus heterozygous
713 controls. We detected serotonin-mediated differences in both the kinetics and amplitude of L2
714 neurons' response to visual stimuli and saw effects on both dark and light flash induced calcium
715 transients in mutants (Fig 6). By contrast, experiments comparing the effects of saline versus
716 serotonin in 5-HT2B +/+ flies showed a significant difference in only one kinetic measurement
717 and only in response to a dark flask (Fig 5). We suggest that the 5-HT2B mutant functioned as a

718 “sensitized genetic background” to enhance the detection of serotonin’s effects and speculate
719 that endogenous serotonergic release and its activation of 5-HT2B may have obscured the
720 effects of bath-applied serotonin in wild type 5-HT2B flies. A saturation point for
721 neuromodulatory input is critical for circuit stability as has been described previously [2, 116,
722 117], and release of endogenous serotonin under the conditions used for these experiments
723 might generate extracellular concentrations near the saturation point for regulating the response
724 of L2 to visual stimuli. In the absence of a functional 5-HT2B receptor, neither endogenous nor
725 exogenous serotonin would have any effect, thus increasing our ability to detect a difference
726 between the 5-HT2B mutant and heterozygous controls (Fig 6). Similarly, the effects of
727 serotonin on pathways mediated by other receptors in the visual system may only become
728 detectable using additional receptor mutants. More generally, we suggest that our data
729 underscore the power of a genetically sensitized background to fully understand the
730 mechanisms underlying the aminergic regulation of circuit function.

731 While the precise function of serotonergic signaling in L2 neurons or elsewhere in the fly
732 visual system remains unknown, it may allow neurons to adapt to changes in visual stimuli. We
733 are struck by the similarities between the changes we observe during perfusion with serotonin
734 and the graded responses of lamina neurons to stimuli of increasing contrast [31]. Changes in
735 calcium levels at the nerve terminal suggests that serotonin might regulate inputs to L2 nerve
736 terminals, or perhaps regulate neurotransmitter release, where increased calcium levels could
737 drive an increase in neurotransmitter release onto postsynaptic neurons. Dissecting these
738 potential mechanisms will require the analysis of neurons downstream of L2, but these too, may
739 undergo direct or indirect serotonergic regulation independent of the effects of serotonin on L2
740 neurons [37, 118, 119]. Studies in mammals have already begun to dissect the contributions of
741 serotonergic tuning in multiple cells within individual circuits including the visual system [6, 18,
742 23, 120, 121] but the way in which this information is integrated remains poorly understood. The

743 interactions between receptors expressed on L2 and other neurons in the fly visual system
744 provide a new framework to dissect the mechanism by which multiplexed serotonergic inputs
745 combine to regulate circuit function.

746

747 **Conclusion**

748 In this study we confirm that several cells in the *Drosophila* optic lobe express specific
749 serotonin receptor subtypes. We then demonstrate that subsets of neurons involved in the initial
750 steps of visual processing are regulated by serotonin through both presumptive cell autonomous
751 and non-autonomous mechanisms. These data established a new platform to study the cellular
752 mechanisms by which serotonin regulates sensory circuits.

753

754

755 **Supporting Information Legends**

756 **S1 Fig. Serotonin receptors and serotonergic projections in the optic lobe**. (**A-H**)
757 Serotonin receptor MiMIC-T2A-GAL4 lines were crossed to UAS-mCD8::RFP (visualized here in
758 green) to identify patterns of expression in the optic lobe. (**A**) A schematic of the optic lobe
759 neuropils including the lamina (la), medulla (me), lobula (lo) and lobula plate (lp) with the
760 neuropil in grey and the cortex containing neuronal cell bodies in white. (**B-F**) Neuropil is labeled
761 by anti-N-Cadherin staining (blue) to provide anatomical reference for labeled cells (green)
762 representing 5-HT1A (**B**), 5-HT1B (**C**), 5-HT2A (**D**), 5-HT2B (**E**), and 5-HT7 (**F**). MiMIC-T2A-
763 GAL4 line labeled projections were visible in all optic lobe neuropils including the lamina
764 neuropil, which is enlarged in (B'), (C'), (E') and (F'). N=4-8 and scale bars are 20 μm.

765 **S2 Fig. Data sets reporting evidence of serotonin receptor expression in optic lobe**
766 **neurons.** The current study includes MiMIC-T2A-GAL4>MCFO for identification based on
767 morphology (green) and FACS-SMART-Seq of L2 and T1 neurons (blue). Davis et al. 2020
768 employed TAPIN-Seq and reported probability of expressions (GSE116969, Table 7B) for each
769 cell type. Serotonin receptor expression with a p>0.75 are shown (purple). Konstantinides et al.
770 2018 used FACS-SMART-Seq for T1, Mi1, C2 and C3 cells (GSE103772). Serotonin receptors
771 with counts greater than 1,000 in at least two replicates are shown (orange).

772 **S3 Fig. Serotonin receptor MiMIC-T2A-GAL4 lines potentially label L2, C2, TMY3, and Mi1**
773 **cells.** (**A**) 5-HT2B-MiMIC-T2A-GAL4>UAS-RFP (green) was combined with ChAT-MiMIC-
774 LexA>LexAop-GFP (magenta). Co-labeling was observed in cell bodies in the lamina cortex,
775 shown in insets (arrowheads). (**B-C**) 5-HT7-MiMIC-T2A-GAL4 labeled cells with a morphology

similar to lamina monopolar cell 5 (L5). (**D**) 5-HT1A-MiMIC-T2A-GAL4>MCFO labeled C2-like cells in the lamina neuropil. (**E**) Colocalization was observed between 5-HT1A MiMIC-T2A-GAL4 and GAD1 MiMIC-T2A-LexA in the lamina neuropil and cell bodies adjacent to the lobula plate (arrowhead, E). (**F-G**) 5-HT7-MiMIC-GAL4>MCFO (F) and 5-HT1A-MiMIC-T2A-GAL4>MCFO (G) labeled cells with morphology similar to TmY3. (**H**) 5-HT7-MiMIC-GAL4>MCFO also labeled cells that resembled Mi1. For co-labeling in (A) and (E), N=4-8 brains per condition. For MCFO, L5-like cells in (B-C) were observed in 7/13 brains, C2 cells in (D) were observed in 3/31 brains, TMY3 cells in (F) were observed in 4/13 brains, TmY3 cells in (G) were observed in 5/31 brains and Mi1 cells in (H) were observed in 6/13 brains. Scale bars are 20 μm for (A, D-H) and 10 μm for (B-C).

S4 Fig. 5-HT2A labeling in lamina cortex may represent glia cells. (**A**) 5-HT2A-GAL4>MCFO epitopes V5 (green) and HA (magenta) label unidentified cells confined the distal lamina cortex. (**B**) 5-HT2A-T2A-GAL4>UAS-mCD8::GFP (green) labels cells in the lamina cortex in close proximity to nuclei labeled with repo antibody (magenta). Neuropil is labeled by anti-N-Cadherin staining (blue) to provide anatomical reference. N=18 brains for (A) and N=4 brains from (B). Scale bars are 20 um.

S5 Fig. Serotonin receptor 5-HT1B co-labels with serotonin immunoreactive sites in optic lobe and cell bodies in the central brains. Anti-serotonin immunolabeling (magenta) was used to identify serotonergic cells and projections in (A-F). (**A**) Serotonin immunoreactive sites (magenta) were visible in the optic lobe neuropils: lamina (la), medulla (me), lobula (lo) and lobula plate (lp). (**A'-A" and C-C"**) 5-HT1B-MiMIC-T2A-GAL4>UAS-mCD8::GFP labeled cells throughout the optic lobe with close apposition to serotonergic boutons. A neuron in serotonergic cell cluster LP2 is also labeled by 5-HT1B driven GFP (arrowhead, A-A"). (**B**) A schematic of the optic lobe and its major neuropils. (**E-E"**) Serotonin receptor MiMIC-T2A-GAL4 lines were crossed to UAS-MCFO-1 to label individual cells. Using 5-HT1B-MiMIC-T2A-GAL4>MCFO (green), we observed co-labeling between MCFO-labeled cells and serotonergic boutons (magenta) processes in the inner medulla (iM), medulla layer 4 (M4), and lobula (lo). (**D**) A schematic of the fly brain with dashed lines showing the approximate anatomical locations for (C) and (E). (**F-F"**) Anti-serotonin immunolabeling (magenta) co-labeled with 5-HT1B-MiMIC-T2A-GAL4>UAS-mCD8::GFP labeled cell bodies in the central brain. 5-HT1B-labeled kenyon cells (KC) are labeled for anatomical reference in (F"). (**G**) The approximate anatomical location for images in (F-F") are shown in the boundaries of the dashed line. Serotonin co-labeling was performed N=5 for 5-HT1B>GFP (A-A", C-C", and F-F") and N=6 brains for 5-HT1B>MCFO (E-E"). Scale bars are 20 μm.

S6 Fig. Serotonin receptor 5-HT1A co-labels with serotonin immunoreactive sites in optic lobe and cell bodies in the central brain. (**A**) Schematic of the optic lobe neuropils—lamina (la), medulla (me), lobula (lo) and lobula plate (lp)—and serotonergic PLP cells. (**B-B"**) 5-HT1A-MiMIC-T2A-GAL4 driving UAS-mCD8::GFP (green) was co-stained with anti-serotonin immunolabeling (magenta) to map potential autoreceptors to specific cell clusters in the central brain. PLP neurons co-labeling for 5-HT1A labeling and anti-serotonin immunolabeling are indicated by the arrowhead. (**C-E**) Anterior to posterior images taken in the same brain show several serotonergic cell clusters expressing 5-HT1A (labeled at arrowheads). 5-HT1A-labeled mushroom body (MB) and kenyon cells (KC) are labeled for anatomical reference in (**C** and **E**).

819 (**F**) A cartoon of the fly brain with dashed lines to indicate the approximate anatomical location
820 for (C-E). Scale bars are 20 μm and N=6.

821 **S7 Fig. RT-qPCR shows L2 neurons express 5-HT2B and T1 neurons express both**
822 **5-HT1A and 5-HT1B serotonin receptors.** Enrichment (i.e., fold change) was calculated for
823 cDNA from GFP-labeled cell isolates relative to pooled, unlabeled optic lobe cell isolates using
824 the comparative CT method. (**A**) RT-qPCR performed on cDNA from isolated T1 neurons
825 expressing GFP showed enrichment for serotonin receptors 5-HT1A and 5-HT1B relative to
826 other GFP-negative cells from the optic lobe. (**B**) FACS isolates from L2 cells showed
827 enrichment of 5-HT2B and 5-HT7 in RT-qPCR. (**C**) L1 RT-qPCR enrichment was not detectable
828 for any serotonin receptors. RT-qPCR error bars represent mean±SEM. N=3-6 biological
829 replicates pooled from 18-40 brains per replicate.

830 **S8 Fig**. **Serotonergic neurons do not show sybGRASP signal with postsynaptic T1, L2 or**
831 **L1 neurons in the medulla.** SybGRASP was used to probe whether serotonergic neurons
832 make synaptic contacts onto L2, T1 or L1 neurons. L2 neurons are known to synapse onto T1
833 projections in the medulla and we used this connection as a positive control. (**A-A'**) SybGRASP
834 was observed with L2 split-GAL4 presynaptic to T1-LexA in M2. The dashed inset in (**A**) is
835 shown in (**A'**). (**B-E**) A SerT-GAL4 driver was used to express the pre-synaptic portion of GFP in
836 serotonergic neurons and LexA drivers were used to express the postsynaptic portion of GFP in
837 L2 (**B-C**) L1 (**D**) or T1 (**E**) as indicated. No sybGRASP signal was detected in the medulla when
838 SerT was presynaptic to L2 (**B**) however, occasional sparse GFP puncta (arrowhead) were
839 visible in the lamina (**C**). When SerT-GAL4 neurons were presynaptic to L1 (**D**) or T1 (**E**)
840 neurons, we did not detect a sybGRASP signal in either the lamina or medulla. All tissue was
841 labeled with primary antibodies to both 5-HT (magenta) and GFP (green). N=7-10 brains. Scale
842 bars are 15 μm (**A**, **B**, **D-E**); 5 μm (**A"** and **C-C"**).

843 **S9 Fig. Individual traces for serotonin bath application experiments.** (**A-D**) Individual traces
844 representing all experiments (Fig 4) for serotonin or saline controls with L2, L1 or T1 split-
845 GAL4>GCaMP6f or T1 split-GAL4>ArcLight. For all experiments, the first 60 s of baseline is not
846 shown; traces represent data recorded following a switch to saline with serotonin or saline
847 alone. The length of time for the switch to complete was estimated to be 105 s, but the first 60 s
848 of the recording are not shown so the switch occurs at 45 s on the x axis in A-D. Saline controls
849 are gray, serotonin exposed preps are colored, and the dark line represents the mean (**A**)
850 L2>GCaMP6f experiments, along with (**B**) L1>GCaMP6f, show an increase in calcium following
851 serotonin application as compared to saline controls (L2, p=00095; L1, p=0.02). (**C, D**) T1 cells
852 show no significant change with either GCaMP6f (**C**) or ArcLight (**D**) relative to saline (p>0.05)
853 For bath application experiments (**A-D**), N=4-8 individual flies.

854 **S1 Table.** RNA-Seq Serotonin Receptor TPMs, averages and standard deviations.

855 **S2 Table.** RT-qPCR Threshold Cycle (CT) measurements and calculated enrichment for FACS-
856 isolated T1, L2, and L1 samples as shown in S7 Fig. Enrichment (i.e., fold change) was
857 calculated for cDNA from GFP-labeled cell isolates relative to pooled, unlabeled optic lobe cell
858 isolates using the comparative CT method.

859 **S3 Table.** Fly strains used in this study.

860 **S4 Table.** RT-qPCR primer sequences and mRNA (cDNA) target information.

861

862

863

864

865

866 **Methods**

867 **Fly Husbandry and Genetic Lines**

868 Flies were maintained on a standard cornmeal and molasses-based agar media with a
869 12:12 hour light/dark cycle at room temperature (22-25°C). All fly strains used in this study are
870 listed in S3 Table. Serotonin receptor MiMIC-T2A-GAL4 lines described in [68] were a gift from
871 Herman Dierick (Baylor College of Medicine), and include 5-HT1A-T2A-GAL4^{MI01468}, 5-HT1A-
872 T2A-GAL4^{MI01140}, 5-HT1A-T2A-GAL4^{MI04464}, 5-HT1B-T2A-GAL4^{MI05213}, 5-HT2A-T2A-GAL4 ^{MI0459},
873 5-HT2A-GAL4^{MI03299}, 5-HT2B-T2A-GAL4^{MI06500}, 5-HT2B-T2A-GAL4^{MI5208}, 5-HT2B-GAL4^{MI7403},
874 and 5-HT7-GAL4 ^{MI00215}. L1 and T1 split-GAL4 lines [82], as well as unpublished LexA lines for
875 L1 and T1, were provided by Aljoscha Nern (HHMI/Janelia Research Campus). S.L. Zipursky
876 (UCLA) generously provided L2-split-GAL4 and L2-LexA (RRID:BDSC_52510). Yi Rao (Peking
877 University) generously shared 5-HT2B-KO-GAL4 SII (5-HT2B mutant) [85], 5-HT1A::sfGFP [84],
878 and UAS-5-HT2B::sfGFP [85].

879 SerT-GAL4 (RRID:BDSC_38764), GAD1 Trojan LexA (RRID:BDSC_60324) and ChAT
880 Trojan LexA (RRID:BDSC_60319) were obtained from Bloomington *Drosophila* Stock Center
881 (BDSC) at Indiana University (Bloomington, IN, USA). Additional reporters from BDSC include:
882 UAS-mCD8::GFP (RRID:BDSC_5137), UAS-MCFO-1 (RRID:BDSC_64085), UAS-GCaMP6f
883 (RRID:BDSC_42747), UAS-ArcLight (RRID:BDSC_51056), UAS-mCD8::RFP, LexAop-
884 mCD8::GFP (RRID:BDSC_32229), and UAS-nSyb::GFP1-10, LexAop-CD4:GFP11
885 (RRID:BDSC_64314; provided through S.L. Zipursky (UCLA)).

886 **S3 Table.** Animal strains used in this study.

887 **Immunofluorescent Labeling and Imaging**

888 Flies were dissected 5-10 days after eclosion, and equal numbers of males and females
889 were used for all experiments unless otherwise noted. Brains were dissected in ice-cold PBS

890 (Alfa Aesar, Cat#J62036, Tewksbury, MA), then fixed in 4% paraformaldehyde (FisherScientific,
891 Cat#50-980-493, Waltham, MA) in PBS with 0.3% Triton X-100 (Millipore Sigma, Cat#X100,
892 Burlington, MA) (PBST) for one hour at room temperature. After fixation, brains were washed
893 three times with PBST for 10 minutes, then blocked for 30 minutes in PBST containing 0.5%
894 normal goat serum (NGS) (Cayman Chemical, Cat#10006577, Ann Arbor, MA). Antibodies were
895 diluted in 0.5% NGS/PBST. Primary antibodies were incubated with the tissue overnight at 4°C.
896 The next day, the brains were washed three times with PBST for 10 minutes, then incubated
897 with secondary antibodies for 2 hours in the dark at room temperature. Brains were washed
898 three times with PBST for 10 minutes before mounting.

899 For frontal mounting, brains were washed with 60% and 80% glycerol (Millipore Sigma,
900 Cat#G5516) and mounted in Fluoromount-G (SouthernBiotech, Cat#0100-01, Birmingham, AL).
901 For dorsal-ventral mounting, brains were fixed in 2% PFA/PBST overnight. The next day, brains
902 were washed three times with PBST. Brains were dehydrated with a series of 10 min ethanol
903 baths of increasing concentrations (30%, 50%, 75%, 95%, 100%, 100%, and 100%). Brains
904 were then transferred to 100% xylene before mounting in DPX (FisherScientific, Cat#50-980-
905 370).

906 Serotonin immunolabeling was performed with 1:25 rat anti-serotonin (Millipore Sigma,
907 Cat#MAB352, RRID:AB_11213564), 1:1000 rabbit anti-serotonin (ImmunoStar, Cat#20080,
908 Hudson, WI ,RRID:AB_572263) or 1:1000 goat anti-serotonin (ImmunoStar, Cat#20079,
909 RRID:AB_572262). Where noted, GFP was labeled with 1:250 mouse anti-GFP (Sigma-Aldrich,
910 Cat#G6539, RRID:AB_259941; or, ThermoFisher, Waltham, MA, Cat#A-11120,
911 RRID:AB_221568). Secondary antibodies were used at 1:400 and include: Donkey anti-mouse
912 Alexa Fluor 488, Donkey anti-Rabbit Alexa Fluor 594 or Alexa Fluor Donkey anti-rat 647
913 (Jackson ImmunoResearch Laboratories, Westgrove, PA, Cat#715-545-151, # 711-585-152, #
914 712-605-153) or Alexa Fluor 555 (Life Technologies, ThermoFisher, Cat#A-21428).

915 When serotonin receptor MiMIC-GAL4 lines were combined with ChAT or GAD1 MiMIC-
916 LexA (S3 Fig), brains were processed and imaged as described in Sizemore and Dacks 2016
917 [122]. MultiColor FlpOut (MCFO-1) sparse labeling was induced by heat activation at 37°C for
918 10-15 minutes at least 2 days prior to dissection as described [73]. Primary antibodies included
919 1:300 rabbit anti-HA (Cell Signaling Technology, Cat#3724, Danvers, MA, RRID:AB_1549585),
920 1:150 rat anti-FLAG (Novus, Littleton, CA, Cat#NBP1-06712, RRID:AB_1625982), and 1:400
921 mouse anti-V5::Dylight-550 (Bio-Rad, Hercules, CA, Cat#MCA1360D550GA,
922 RRID:AB_2687576). The rat anti-N-Cadherin (DN-Ex#8) and mouse anti-repo (8D12
923 concentrate) was obtained from the Developmental Studies Hybridoma Bank, created by the
924 NICHD of the NIH and maintained at The University of Iowa, Department of Biology, Iowa City,
925 IA 52242. Secondary antibodies used for MCFO are listed above. N-Synaptobrevin GFP
926 Reconstitution Across Synaptic Partners (sybGRASP) flies [86] were dissected, fixed and
927 immunolabeled as described above, without KCl induction. The tissue was labeled with mouse
928 antiserum specific to reconstituted GFP (1:250; Sigma-Aldrich, Cat#G6539, RRID:AB_259941)
929 [123] and either anti-serotonin (antibodies listed above).

930 Imaging was performed with a Zeiss LSM 880 Confocal with Airyscan (Zeiss,
931 Oberkochen, Germany) using a 40x water or 63x oil immersion objective. Post-hoc processing
932 of images was done with Fiji [125] or Adobe Photoshop (Adobe, San Jose, CA) .

933

934 **FACs and RNA Extraction**

935 L2 and L1 neurons were labeled using split-GAL4 drivers combined with UAS-
936 mCD8::GFP (RRID:BDSC_5137). For RNA-Seq in Fig 2, N=3 T1-LexA samples were tested.
937 For RT-qPCR in S7 Fig, we included N=3 T1-split-GLA4 samples and N=3 T1-LexA samples.
938 Brains were dissected on the day of eclosion and optic lobes were dissociated according to

939 previously published methods [126]. The dissociated optic lobe cells were separated by
940 fluorescence-activated cell sorting (FACS) into GFP-positive and GFP-negative isolates using a
941 BD FACS Aria II high-speed cell sorter in collaboration with the UCLA Jonsson Comprehensive
942 Cancer Center (JCCC) and Center for AIDS Research Flow Cytometry Core Facility
943 (http://cyto.mednet.ucla.edu/home.html). For FACS, each experiment was performed with 18-40
944 brains, and yielded between 1,700-7,800 GFP^+ cells. RNA was extracted from isolated cells with
945 ARCTURUS® PicoPure® RNA Isolation Kit (ThermoFisher, KIT0204) or RNeasy Plus Micro Kit
946 (QIAGEN, 74034).

947

948 **RT-qPCR**

949 RNA extracted from FACS isolates was reverse transcribed using SuperScript III
950 (Invitrogen, ThermoFisher, Cat#18080093). RT-qPCR was performed for receptor cDNA using
951 validated primers (S4 Table) and SYBR Green Power PCR Mix (Applied Biosystems,
952 ThermoFisher) on an iQ5 real-time qPCR detection system (Bio-Rad). Primers were designed
953 using Primer-Blast (https://www.ncbi.nlm.nih.gov/tools/primer-blast/) or were from the DGRC
954 FlyPrimerBank [127]; oligonucleotides were obtained from Integrated DNA Technologies
955 (Coralville, Iowa). Primer pairs were validated to amplify a single product, verified by a single
956 melting temperature and single band on an electrophoresis gel. The efficiency for each primer
957 pair was between 85-115%. Comparisons between GFP^+ and GFP^- samples were calculated as
958 enrichment (i.e., fold change) using the comparative CT method [83]. A zero value was imputed
959 for samples with no amplification (i.e., no CT value). Raw CT values are shown in S2 Table.

960

961 **RNA-Seq**

962 RNA-Seq was performed using a SMART-Seq protocol adapted from [126, 128, 129].
963 Libraries were constructed using the SMART-seq v4 Ultra Low-input RNA sequencing kit with
964 Nextera XT (Takara Bio). Paired-end sequencing was conducted by the UCLA genomic core
965 facility (https://www.semel.ucla.edu/ungc/services). After demultiplexing, we obtained between
966 39-270 (average 105) million reads per sample. Quality control was performed on base qualities
967 and nucleotide composition of sequences. Alignment to the *Drosophila melanogaster* genome
968 (BDGP6) was performed using the STAR spliced read aligner [130] with default parameters.
969 Additional QC was performed after the alignment to examine the following: level of mismatch
970 rate, mapping rate to the whole genome, repeats, chromosomes, and key transcriptomic regions
971 (exons, introns, UTRs, genes). Between 75-85% of the reads mapped uniquely to the fly
972 genome. Total counts of read fragments aligned to candidate gene regions within the reference
973 gene annotation were derived using HTSeq program and used as a basis for the quantification
974 of gene expression. Only uniquely mapped reads were used for subsequent analyses. Following
975 alignment and read quantification, we performed quality control using a variety of indices,
976 including consistency of replicates and average gene coverage. For Fig 2, L2 samples were run
977 in two separate sequencing runs and we did not perform corrections for any potential batch
978 effects. Data is shown as Transcripts Per Million (TPMs).

979

980 **Live Cell Imaging**

981 Calcium imaging was performed as previously described [131]. Briefly, flies were
982 anesthetized at 4°C and placed into a chemically etched metal shim within a larger custom-built
983 fly holder. The fly holder was based on a previously described design [132]. The head capsule
984 and the thorax were glued to the metal shim using UV-curable glue (www.esslinger.com). The
985 legs, proboscis and antennae were immobilized using beeswax applied with a heated metal
986 probe (Waxelectric-1, Renfert). The head capsule was immersed in insect saline (103 mM NaCl,

987 3 mM KCl, 1.5mM CaCl2, 4 mM MgCl2, 26 mM NaHCO3, 1 mM NaH2PO4, 10 mM trehalose,
988 10 mM glucose, 5 mM TES, 2 mM sucrose) [133]. A small window on the right rear head
989 capsule was opened using sharp forceps (Dumont, #5SF). Muscles and fat covering the optic
990 lobe were cleared before placing the fly under the 2-photon microscope (VIVO, 3i: Intelligent
991 Imaging Innovations, Denver, CO). Neurons expressing GCaMP6f were imaged at 920-nm
992 using a Ti:Sapphire Laser (Chameleon Vision, Coherent). Images were acquired at 10-20
993 frames/s for Fig 4 and 25-30 frames/s for Fig 5-6 live imaging. Only female flies were used for
994 live imaging experiments.

995 A custom-built gravity perfusion system was used for bath application of either serotonin
996 or saline control to the fly's exposed optic lobe for Fig 4. For Fig 4 and S9 Fig, the tissue was
997 first perfused with insect saline containing 1μm tetrodotoxin citrate (TTX) (Alomone Labs,
998 Jerusalem, Israel, Cat#T-550) for at least 5 minutes at 2 mL/min, prior to each recording. TTX
999 remained present throughout the experiment. To examine the effects of serotonin on calcium
1000 levels, baseline GCaMP6f fluorescence was recorded for one minute before switching to the
1001 second input containing either 100μM serotonin hydrochloride (Sigma Aldrich, Cat# H9523) or
1002 saline alone for an additional five minutes of recording. Due to perfusion tubing length and dead
1003 volume, the perfusion switch took approximately 105 s to reach the tissue. Fig 4 does not show
1004 the first minute of the recording, so the solution switch occurs at approximately 45 s on the x
1005 axis. For more precise control of perfusion solutions, we used a programmable valve controller
1006 (VC-6, Warner Instruments, Hamden, CT) for Fig 5-6 visual experiments (see details below).

1007

1008 **Visual Stimulus Experiments**

1009 Visual stimuli were shown using an arena composed of 48 eight by eight-pixel LED
1010 panels, at 470 nm (Adafruit, NY, NY). The panels were assembled into a curved display that

1011 extends 216° along the azimuth and ±35° in elevation. Each pixel subtended an angle of 2.2° on
1012 the retina at the equatorial axis. To prevent spurious excitation of the imaging photomultiplier
1013 tubes, three layers of blue filter (Rosco no. 59 Indigo) were placed over the LED display.

1014 Each stimulus consisted of a brief increment (light flash) or decrement (dark flash) of the
1015 entire display for 100 ms, before returning to a mid-intensity brightness for 4.9 s. Images were
1016 acquired at 25-30 frames/s for Fig 5-6 visual stimulation experiments. Stimuli were presented in
1017 sets of six bright and six dark flashes randomly shuffled for each minute of the experiment.
1018 Responses were then pooled for each minute. During the first minute ("epoch 1" in Figs 5-6),
1019 and prior to imaging, the tissue was perfused with saline for a baseline recording. At the end of
1020 the first minute, a valve controller (VC-6, Warner Instruments, Hamden, CT) activated by a TTL
1021 signal switched the perfusion to either saline with 100 μM serotonin or saline alone; imaging
1022 then continued for an additional five minutes, for a total of one baseline set and five post-switch
1023 sets of stimuli. The perfusion switch took approximately 45 s to reach the tissue using the
1024 programmable valve system.

1025 **Analysis**

1026 Calcium imaging data were analyzed with Matlab R2017a (Mathworks, Natick, MA). Post
1027 hoc, recordings were corrected for movement of the brain within the imaging plane using a
1028 custom algorithm [134]. Regions of interest (ROIs) were found semi-automatically for data in
1029 Figs 4-6: first, the median intensity of all pixels across all image frames was found; this value
1030 was used as a threshold and all pixels with mean intensity below the threshold, typically within
1031 the image background, were discarded. The 1-D time series of intensity for each remaining pixel
1032 was then extracted. K-means clustering was used to identify pixels with similar activity over the
1033 course of the experiment: three clusters were identified and the cluster with the highest number
1034 of pixels was retained. This reliably identified the pixels within active neurons in the imaging
1035 data and aided in identifying preparations with out-of-plane movement, which were discarded.

1036 For baseline activity experiments (Fig 4), the remaining cluster was used as a single ROI
1037 and the mean intensity within the ROI was found for each image frame to produce a single time-
1038 series for the entire experiment. For visual response experiments (Figs 5-6), pixels within the
1039 remaining cluster were automatically divided into groups corresponding to individual L2
1040 terminals using a watershed transform. The mean intensity within each ROI was found for each
1041 image frame to produce a single time-series for the entire experiment, and the time-series for all
1042 terminal ROIs within an individual animal were then averaged. For Fig 6, ROIs of L2 terminals
1043 were first identified automatically, as above, then manually selected individually according to
1044 layer position because the 5-HT2B GAL4 SII mutant line labeled other cells in addition to L2
1045 neurons.

1046 Approximately half of the bath application recordings showed oscillations in activity due
1047 to slow, periodic movement of the brain at around 0.04 Hz; we applied a second-order notch
1048 filter at this frequency with a bandwidth of 0.005 Hz to remove these oscillations. For the bath
1049 application experiments (Fig 4), we plotted $\Delta F/F$, defined as $(F_t-F_0)/F_0$, where F_t is the mean
1050 fluorescence in the ROI at the indicated time and F_0 is the mean value of F_t during 60 seconds
1051 of baseline activity at the beginning of the experiment and prior to the change in perfusion. For
1052 the visual stimulus experiments (Figs 5-6), we again plotted $\Delta F/F$, defined as $(F_t-F_0)/F_0$, where F_t
1053 is the mean fluorescence across all individual terminal ROIs at the indicated time and F_0 is the
1054 mean of 30 seconds of non-consecutive baseline activity between stimulus presentations during
1055 epoch 1 at the beginning of the experiment and prior to the change in perfusion (Fig 5A). For the
1056 stimulus response plots (Figs 5B, D, 6C, E), we found the average $\Delta F/F$ time-series within each
1057 epoch for each fly after subtracting the average pre-stimulus baseline activity level (0.5 s
1058 preceding each flash stimulus) from each time-series, so that all responses started aligned at 0
1059 $\Delta F/F$. For further analysis (Figs 5C, E, 6D, F), we found the changes in response amplitude
1060 across epochs, defined for the dark stimulus presentation (top) as the difference between the

1061 pre-stimulus baseline and the maximum ΔF/F value that occurred up to 1.75 s after cessation of
1062 the 0.1 s flash, and for the light stimulus (bottom) as the minimum ΔF/F value that occurred in
1063 the same period of time. For each epoch, we subtracted the value of the responses during
1064 epoch 1 at the beginning of the experiment and prior to the change in perfusion, in order to find
1065 the change in amplitude relative to epoch 1. We followed a similar procedure for the analysis of
1066 peak-peak time (Figs 5C', E', 6D', F'), defined as the length of time between the minimum and
1067 maximum ΔF/F values that occurred within 1.75 s after cessation of the 0.1 s flash. The slope of
1068 the transient decay was also calculated (Figs 5C", E", 6D", F").

1069 To examine the baseline changes in fluorescence in visual experiments shown in Figs
1070 6A-B responses to the visual stimuli were removed using a series of second-order notch filters
1071 at 0.19-0.21 Hz and 0.38-0.42 Hz.

1072 **Statistical Tests**

1073 For Fig 5 (C-C", E-E") and Fig 6 (D-D", E-E") comparisons are two-way repeated
1074 measure ANOVA (brackets show interactions between time and genotype) and Sidak's multiple
1075 comparisons tests, $p \leq 0.05$ *, $p \leq 0.01$**, $p \leq 0.001$***, $p \leq 0.0001$****. These tests were performed
1076 using Graphpad Prism Software (San Diego, CA). Differences in baseline calcium shown in Fig
1077 6A-B were calculated by two-tailed Wilcoxon rank sum tests in Matlab R2017a.

1078 **Replicates**

1079 Each biological replicate (N) represents one fly, except for RT-qPCR and RNA-Seq (Fig
1080 2, and S7 Fig E) where each biological replicate was pooled from 18+ flies. RT-qPCR
1081 experiments include 3 technical replicates, which are averaged to represent a single biological
1082 replicate. Animals from at least 3 crosses were used for each experiment. Data for each
1083 experiment was collected over 2-6 months in at least 3 experiments. No outliers were removed

1084 from any data set. Live imaging recordings with too much movement were excluded and not
1085 analyzed.

1086

1087 **Acknowledgements:** We thank members of Larry Zipursky's lab (UCLA) including Elizabeth
1088 Zuniga Sanchez, Liming Tan, and Juyoun Yoo for advice on FACS, RNA extraction, RT-qPCR
1089 and SMART-Seq. Thank you to Deanne Umbay (Brown University) and Nikoo Dalili (UCLA) for
1090 their assistance. We thank members of the Frye and Krantz labs for helpful discussions, and
1091 Aljoscha Nern (HHMI/Janelia Research Campus) and Herman Dierick (Baylor) for generously
1092 supplying fly lines.

1093

1094 **Funding:** This work was funded by R01 MH107390 (DEK), R01 MH114017 (DEK) R01
1095 EY026031 (MAF), IOS-1455869 (MAF), R03 DC013997 (AMD), R01 DC016293 (AMD) and a
1096 seed grant from the UCLA Depression Grand Challenge (DEK, MAF). MMS was supported by a
1097 National Science Foundation GRFP, UCLA Cota-Robles fellowship and F99 NS113454. TRS
1098 was supported by a Grant-In-Aid of Research (G20141015669888) from Sigma Xi, The
1099 Scientific Research Society.

1100 **Competing interests:** The authors deny any relevant paid employment or consultancy, stock
1101 ownership, patent applications, personal relationships with relevant individuals, or membership
1102 of an advisory board.

1103

1104 **References**

1105 1. Kupfermann I. Modulatory actions of neurotransmitters. Annual review of neuroscience.
1106 1979;2:447-65. doi: 10.1146/annurev.ne.02.030179.002311. PubMed PMID: 44174.
1107 2. Marder E. Neuromodulation of neuronal circuits: back to the future. Neuron.
1108 2012;76(1):1-11. doi: 10.1016/j.neuron.2012.09.010. PubMed PMID: 23040802; PubMed
1109 Central PMCID: PMC3482119.
1110 3. Marder E, O'Leary T, Shruti S. Neuromodulation of circuits with variable parameters:
1111 single neurons and small circuits reveal principles of state-dependent and robust
1112 neuromodulation. Annual review of neuroscience. 2014;37:329-46. doi: 10.1146/annurev-neuro-
1113 071013-013958. PubMed PMID: 25032499.
1114 4. Nadim F, Bucher D. Neuromodulation of neurons and synapses. Current opinion in
1115 neurobiology. 2014;29:48-56. doi: 10.1016/j.conb.2014.05.003. PubMed PMID: 24907657;
1116 PubMed Central PMCID: PMC4252488.
1117 5. Katz PS. Beyond neurotransmission : neuromodulation and its importance for
1118 information processing. Osford ; New York: Oxford University Press; 1999. xiii, 391 p. p.
1119 6. Moreau AW, Amar M, Le Roux N, Morel N, Fossier P. Serotoninergic fine-tuning of the
1120 excitation-inhibition balance in rat visual cortical networks. Cereb Cortex. 2010;20(2):456-67.
1121 Epub 2009/06/11. doi: 10.1093/cercor/bhp114. PubMed PMID: 19520765.
1122 7. Arechiga H, Banuelos E, Frixione E, Picones A, Rodriguez-Sosa L. Modulation of
1123 crayfish retinal sensitivity by 5-hydroxytryptamine. The Journal of experimental biology.
1124 1990;150:123-43. PubMed PMID: 2355208.
1125 8. Seillier L, Lorenz C, Kawaguchi K, Ott T, Nieder A, Pourriahi P, et al. Serotonin
1126 Decreases the Gain of Visual Responses in Awake Macaque V1. The Journal of neuroscience :
1127 the official journal of the Society for Neuroscience. 2017;37(47):11390-405. doi:
1128 10.1523/JNEUROSCI.1339-17.2017. PubMed PMID: 29042433; PubMed Central PMCID:
1129 PMC5700422.
1130 9. Kloppenburg P, Ferns D, Mercer AR. Serotonin enhances central olfactory neuron
1131 responses to female sex pheromone in the male sphinx moth manduca sexta. The Journal of
1132 neuroscience : the official journal of the Society for Neuroscience. 1999;19(19):8172-81.
1133 PubMed PMID: 10493719.
1134 10. Dacks AM, Christensen TA, Hildebrand JG. Modulation of olfactory information
1135 processing in the antennal lobe of Manduca sexta by serotonin. Journal of neurophysiology.
1136 2008;99(5):2077-85. doi: 10.1152/jn.01372.2007. PubMed PMID: 18322001.
1137 11. Lottem E, Lorincz ML, Mainen ZF. Optogenetic Activation of Dorsal Raphe Serotonin
1138 Neurons Rapidly Inhibits Spontaneous But Not Odor-Evoked Activity in Olfactory Cortex. The
1139 Journal of neuroscience : the official journal of the Society for Neuroscience. 2016;36(1):7-18.
1140 doi: 10.1523/JNEUROSCI.3008-15.2016. PubMed PMID: 26740645.
1141 12. Brunert D, Tsuno Y, Rothermel M, Shipley MT, Wachowiak M. Cell-Type-Specific
1142 Modulation of Sensory Responses in Olfactory Bulb Circuits by Serotonergic Projections from
1143 the Raphe Nuclei. The Journal of neuroscience : the official journal of the Society for
1144 Neuroscience. 2016;36(25):6820-35. doi: 10.1523/JNEUROSCI.3667-15.2016. PubMed PMID:
1145 27335411; PubMed Central PMCID: PMC4916254.
1146 13. Petzold GC, Hagiwara A, Murthy VN. Serotonergic modulation of odor input to the
1147 mammalian olfactory bulb. Nature neuroscience. 2009;12(6):784-91. doi: 10.1038/nn.2335.
1148 PubMed PMID: 19430472.
1149 14. Papesh MA, Hurley LM. Modulation of auditory brainstem responses by serotonin and
1150 specific serotonin receptors. Hearing research. 2016;332:121-36. doi:
1151 10.1016/j.heares.2015.11.014. PubMed PMID: 26688176.

1152 15. Fotowat H, Harvey-Girard E, Cheer JF, Krahe R, Maler L. Subsecond Sensory
1153 Modulation of Serotonin Levels in a Primary Sensory Area and Its Relation to Ongoing
1154 Communication Behavior in a Weakly Electric Fish. eNeuro. 2016;3(5). doi:
1155 10.1523/ENEURO.0115-16.2016. PubMed PMID: 27844054; PubMed Central PMCID:
1156 PMC5093153.
1157 16. Andres M, Seifert M, Spalthoff C, Warren B, Weiss L, Giraldo D, et al. Auditory Efferent
1158 System Modulates Mosquito Hearing. Current biology : CB. 2016;26(15):2028-36. doi:
1159 10.1016/j.cub.2016.05.077. PubMed PMID: 27476597.
1160 17. Watakabe A, Komatsu Y, Sadakane O, Shimegi S, Takahata T, Higo N, et al. Enriched
1161 expression of serotonin 1B and 2A receptor genes in macaque visual cortex and their
1162 bidirectional modulatory effects on neuronal responses. Cereb Cortex. 2009;19(8):1915-28. doi:
1163 10.1093/cercor/bhn219. PubMed PMID: 19056862; PubMed Central PMCID: PMC2705701.
1164 18. Gagolewicz PJ, Dringenberg HC. Age-Dependent Switch of the Role of Serotonergic 5-
1165 HT1A Receptors in Gating Long-Term Potentiation in Rat Visual Cortex In Vivo. Neural Plast.
1166 2016;2016:6404082. Epub 2016/05/10. doi: 10.1155/2016/6404082. PubMed PMID: 27247804;
1167 PubMed Central PMCID: PMCPMC4877497.
1168 19. Lombaert N, Hennes M, Gilissen S, Schevenels G, Aerts L, Vanlaer R, et al. 5-HTR2A
1169 and 5-HTR3A but not 5-HTR1A antagonism impairs the cross-modal reactivation of deprived
1170 visual cortex in adulthood. Mol Brain. 2018;11(1):65. Epub 2018/11/06. doi: 10.1186/s13041-
1171 018-0404-5. PubMed PMID: 30400993; PubMed Central PMCID: PMCPMC6218970.
1172 20. Gu Q, Singer W. Involvement of serotonin in developmental plasticity of kitten visual
1173 cortex. Eur J Neurosci. 1995;7(6):1146-53. PubMed PMID: 7582087.
1174 21. Wang Y, Gu Q, Cynader MS. Blockade of serotonin-2C receptors by mesulergine
1175 reduces ocular dominance plasticity in kitten visual cortex. Exp Brain Res. 1997;114(2):321-8.
1176 PubMed PMID: 9166921.
1177 22. Shimegi S, Kimura A, Sato A, Aoyama C, Mizuyama R, Tsunoda K, et al. Cholinergic
1178 and serotonergic modulation of visual information processing in monkey V1. Journal of
1179 physiology, Paris. 2016;110(1-2):44-51. doi: 10.1016/j.jphysparis.2016.09.001. PubMed PMID:
1180 27619519.
1181 23. Zhou X, Zhang R, Zhang S, Wu J, Sun X. Activation of 5-HT1A receptors promotes
1182 retinal ganglion cell function by inhibiting the cAMP-PKA pathway to modulate presynaptic
1183 GABA release in chronic glaucoma. The Journal of neuroscience : the official journal of the
1184 Society for Neuroscience. 2018. Epub 2018/12/12. doi: 10.1523/JNEUROSCI.1685-18.2018.
1185 PubMed PMID: 30541912.
1186 24. Trakhtenberg EF, Pita-Thomas W, Fernandez SG, Patel KH, Venugopalan P, Shechter
1187 JM, et al. Serotonin receptor 2C regulates neurite growth and is necessary for normal retinal
1188 processing of visual information. Developmental neurobiology. 2017;77(4):419-37. doi:
1189 10.1002/dneu.22391. PubMed PMID: 26999672.
1190 25. Borst A, Helmstaedter M. Common circuit design in fly and mammalian motion vision.
1191 Nature neuroscience. 2015;18(8):1067-76. doi: 10.1038/nn.4050. PubMed PMID: 26120965.
1192 26. Cheng KY, Frye MA. Neuromodulation of insect motion vision. Journal of comparative
1193 physiology A, Neuroethology, sensory, neural, and behavioral physiology. 2019. doi:
1194 10.1007/s00359-019-01383-9. PubMed PMID: 31811398.
1195 27. Meinertzhagen IA, O'Neil SD. Synaptic organization of columnar elements in the lamina
1196 of the wild type in Drosophila melanogaster. The Journal of comparative neurology.
1197 1991;305(2):232-63. doi: 10.1002/cne.903050206. PubMed PMID: 1902848.
1198 28. Joesch M, Schnell B, Raghu SV, Reiff DF, Borst A. ON and OFF pathways in Drosophila
1199 motion vision. Nature. 2010;468(7321):300-4. doi: 10.1038/nature09545. PubMed PMID:
1200 21068841.

1201 29. Strother JA, Nern A, Reiser MB. Direct observation of ON and OFF pathways in the
1202 Drosophila visual system. Current biology : CB. 2014;24(9):976-83. Epub 2014/04/03. doi:
1203 10.1016/j.cub.2014.03.017. PubMed PMID: 24704075.
1204 30. Clark DA, Bursztyn L, Horowitz MA, Schnitzer MJ, Clandinin TR. Defining the
1205 computational structure of the motion detector in Drosophila. Neuron. 2011;70(6):1165-77. doi:
1206 10.1016/j.neuron.2011.05.023. PubMed PMID: 21689602; PubMed Central PMCID:
1207 PMC3121538.
1208 31. Yang HH, St-Pierre F, Sun X, Ding X, Lin MZ, Clandinin TR. Subcellular Imaging of
1209 Voltage and Calcium Signals Reveals Neural Processing In Vivo. Cell. 2016;166(1):245-57.
1210 Epub 2016/06/02. doi: 10.1016/j.cell.2016.05.031. PubMed PMID: 27264607; PubMed Central
1211 PMCID: PMCPMC5606228.
1212 32. Zheng L, de Polavieja GG, Wolfram V, Asyali MH, Hardie RC, Juusola M. Feedback
1213 network controls photoreceptor output at the layer of first visual synapses in Drosophila. The
1214 Journal of general physiology. 2006;127(5):495-510. doi: 10.1085/jgp.200509470. PubMed
1215 PMID: 16636201; PubMed Central PMCID: PMC2151524.
1216 33. Behnia R, Desplan C. Visual circuits in flies: beginning to see the whole picture. Current
1217 opinion in neurobiology. 2015;34:125-32. doi: 10.1016/j.conb.2015.03.010. PubMed PMID:
1218 25881091; PubMed Central PMCID: PMCPMC4577302.
1219 34. Bahl A, Serbe E, Meier M, Ammer G, Borst A. Neural Mechanisms for Drosophila
1220 Contrast Vision. Neuron. 2015;88(6):1240-52. doi: 10.1016/j.neuron.2015.11.004. PubMed
1221 PMID: 26673659.
1222 35. Rivera-Alba M, Vitaladevuni SN, Mishchenko Y, Lu Z, Takemura SY, Scheffer L, et al.
1223 Wiring economy and volume exclusion determine neuronal placement in the Drosophila brain.
1224 Current biology : CB. 2011;21(23):2000-5. doi: 10.1016/j.cub.2011.10.022. PubMed PMID:
1225 22119527; PubMed Central PMCID: PMC3244492.
1226 36. Takemura SY, Lu Z, Meinertzhagen IA. Synaptic circuits of the Drosophila optic lobe: the
1227 input terminals to the medulla. The Journal of comparative neurology. 2008;509(5):493-513. doi:
1228 10.1002/cne.21757. PubMed PMID: 18537121; PubMed Central PMCID: PMC2481516.
1229 37. Takemura SY, Bharioke A, Lu Z, Nern A, Vitaladevuni S, Rivlin PK, et al. A visual motion
1230 detection circuit suggested by Drosophila connectomics. Nature. 2013;500(7461):175-81. doi:
1231 10.1038/nature12450. PubMed PMID: 23925240; PubMed Central PMCID: PMCPMC3799980.
1232 38. Takemura SY, Xu CS, Lu Z, Rivlin PK, Parag T, Olbris DJ, et al. Synaptic circuits and
1233 their variations within different columns in the visual system of Drosophila. Proceedings of the
1234 National Academy of Sciences of the United States of America. 2015;112(44):13711-6. doi:
1235 10.1073/pnas.1509820112. PubMed PMID: 26483464; PubMed Central PMCID: PMC4640747.
1236 39. Takemura SY, Nern A, Chklovskii DB, Scheffer LK, Rubin GM, Meinertzhagen IA. The
1237 comprehensive connectome of a neural substrate for 'ON' motion detection in. Elife. 2017;6.
1238 Epub 2017/04/22. doi: 10.7554/eLife.24394. PubMed PMID: 28432786; PubMed Central
1239 PMCID: PMCPMC5435463.
1240 40. Shinomiya K, Huang G, Lu Z, Parag T, Xu CS, Aniceto R, et al. Comparisons between
1241 the ON- and OFF-edge motion pathways in the Drosophila brain. Elife. 2019;8. doi:
1242 10.7554/eLife.40025. PubMed PMID: 30624205; PubMed Central PMCID: PMC6338461.
1243 41. Wasserman SM, Aptekar JW, Lu P, Nguyen J, Wang AL, Keles MF, et al. Olfactory
1244 neuromodulation of motion vision circuitry in Drosophila. Current biology : CB. 2015;25(4):467-
1245 72. doi: 10.1016/j.cub.2014.12.012. PubMed PMID: 25619767; PubMed Central PMCID:
1246 PMC4331282.
1247 42. Strother JA, Wu ST, Rogers EM, Eliason JLM, Wong AM, Nern A, et al. Behavioral state
1248 modulates the ON visual motion pathway of Drosophila. Proceedings of the National Academy
1249 of Sciences of the United States of America. 2018;115(1):E102-E11. doi:
1250 10.1073/pnas.1703090115. PubMed PMID: 29255026; PubMed Central PMCID: PMC5776785.

1251 43. Cheng KY, Colbath RA, Frye MA. Olfactory and Neuromodulatory Signals Reverse
1252 Visual Object Avoidance to Approach in Drosophila. Current biology : CB. 2019;29(12):2058-65
1253 e2. doi: 10.1016/j.cub.2019.05.010. PubMed PMID: 31155354; PubMed Central PMCID:
1254 PMC6615044.
1255 44. Hevers W, Hardie RC. Serotonin modulates the voltage dependence of delayed rectifier
1256 and Shaker potassium channels in Drosophila photoreceptors. Neuron. 1995;14:845-56.
1257 45. Kloppenburg P, Erber J. The modulatory effects of serotonin and octopamine in the
1258 visual system of the honey bee (Apis mellifera L.) II. Electrophysiological analysis of motion-
1259 sensitive neurons in the lobula. Journal of comparative physiology A, Neuroethology, sensory,
1260 neural, and behavioral physiology. 1995;176:119-29.
1261 46. Suver MP, Mamiya A, Dickinson MH. Octopamine neurons mediate flight-induced
1262 modulation of visual processing in Drosophila. Current biology : CB. 2012;22(24):2294-302. doi:
1263 10.1016/j.cub.2012.10.034. PubMed PMID: 23142045.
1264 47. Leitinger G, Pabst MA, Kral K. Serotonin-immunoreactive neurones in the visual system
1265 of the praying mantis: an immunohistochemical, confocal laser scanning and electron
1266 microscopic study. Brain Res. 1999;823(1-2):11-23. PubMed PMID: 10095007.
1267 48. Nässel DR, Meyer EP, Klemm N. Mapping and ultrastructure of serotonin-
1268 immunoreactive neurons in the optic lobes of three insect species. The Journal of comparative
1269 neurology. 1985;232(2):190-204. doi: 10.1002/cne.902320205. PubMed PMID: 3973090.
1270 49. Nässel DR, Ohlsson L, Sivasubramanian P. Postembryonic differentiation of serotonin-
1271 immunoreactive neurons in fleshfly optic lobes developing in situ or cultured in vivo without eye
1272 discs. The Journal of comparative neurology. 1987;255(3):327-40. doi: 10.1002/cne.902550302.
1273 PubMed PMID: 3546409.
1274 50. Valles AM, White K. Serotonin-containing neurons in Drosophila melanogaster:
1275 development and distribution. The Journal of comparative neurology. 1988;268(3):414-28. doi:
1276 10.1002/cne.902680310. PubMed PMID: 3129459.
1277 51. Hamanaka Y, Kinoshita M, Homberg U, Arikawa K. Immunocytochemical localization of
1278 amines and GABA in the optic lobe of the butterfly, Papilio xuthus. PloS one. 2012;7(7):e41109.
1279 doi: 10.1371/journal.pone.0041109. PubMed PMID: 22844431; PubMed Central PMCID:
1280 PMC3402530.
1281 52. Schafer S, Bicker G. Common projection areas of 5-HT- and GABA-like immunoreactive
1282 fibers in the visual system of the honeybee. Brain Res. 1986;380(2):368-70. PubMed PMID:
1283 3530374.
1284 53. Chen B, Meinertzhagen IA, Shaw SR. Circadian rhythms in light-evoked responses of
1285 the fly's compound eye, and the effects of neuromodulators 5-HT and the peptide PDF. J Comp
1286 Physiol [A]. 1999;185:393-404.
1287 54. Ichikawa T. Light suppresses the activity of serotonin-immunoreactive neurons in the
1288 optic lobe of the swallowtail butterfly. Neurosci Lett. 1994;172(1-2):115-8. PubMed PMID:
1289 8084513.
1290 55. Pyza E, Meinertzhagen IA. Neurotransmitters regulate rhythmic size changes amongst
1291 cells in the fly's optic lobe. Journal of comparative physiology A, Sensory, neural, and
1292 behavioral physiology. 1996;178(1):33-45. doi: 10.1007/bf00189588. PubMed PMID: 8568723.
1293 56. Nichols DE, Nichols CD. Serotonin receptors. Chemical reviews. 2008;108(5):1614-41.
1294 doi: 10.1021/cr078224o. PubMed PMID: 18476671.
1295 57. McCorvy JD, Roth BL. Structure and function of serotonin G protein-coupled receptors.
1296 Pharmacology & therapeutics. 2015;150:129-42. doi: 10.1016/j.pharmthera.2015.01.009.
1297 PubMed PMID: 25601315; PubMed Central PMCID: PMC4414735.
1298 58. Maroteaux L, Bechade C, Roumier A. Dimers of serotonin receptors: Impact on ligand
1299 affinity and signaling. Biochimie. 2019;161:23-33. doi: 10.1016/j.biochi.2019.01.009. PubMed
1300 PMID: 30685449.

1301 59. Araneda R, Andrade R. 5-Hydroxytryptamine2 and 5-hydroxytryptamine 1A receptors
1302 mediate opposing responses on membrane excitability in rat association cortex. Neuroscience.
1303 1991;40(2):399-412. doi: 10.1016/0306-4522(91)90128-b. PubMed PMID: 1851255.
1304 60. Celada P, Puig MV, Artigas F. Serotonin modulation of cortical neurons and networks.
1305 Frontiers in integrative neuroscience. 2013;7:25. doi: 10.3389/fnint.2013.00025. PubMed PMID:
1306 23626526; PubMed Central PMCID: PMC3630391.
1307 61. Davis FP, Nern A, Picard S, Reiser MB, Rubin GM, Eddy SR, et al. A genetic, genomic,
1308 and computational resource for exploring neural circuit function. Elife. 2020;9. doi:
1309 10.7554/eLife.50901. PubMed PMID: 31939737.
1310 62. Konstantinides N, Kapuralin K, Fadil C, Barboza L, Satija R, Desplan C. Phenotypic
1311 Convergence: Distinct Transcription Factors Regulate Common Terminal Features. Cell.
1312 2018;174(3):622-35 e13. Epub 2018/06/19. doi: 10.1016/j.cell.2018.05.021. PubMed PMID:
1313 29909983; PubMed Central PMCID: PMCPMC6082168.
1314 63. Colas JF, Launay JM, Kellermann O, Rosay P, Maroteaux L. Drosophila 5-HT2
1315 serotonin receptor: coexpression with fushi-tarazu during segmentation. Proceedings of the
1316 National Academy of Sciences of the United States of America. 1995;92(12):5441-5. PubMed
1317 PMID: 7777527; PubMed Central PMCID: PMC41710.
1318 64. Gasque G, Conway S, Huang J, Rao Y, Vosshall LB. Small molecule drug screening in
1319 Drosophila identifies the 5HT2A receptor as a feeding modulation target. Scientific reports.
1320 2013;3:srep02120. doi: 10.1038/srep02120. PubMed PMID: 23817146; PubMed Central
1321 PMCID: PMC3698492.
1322 65. Saudou F, Boschert U, Amlaiky N, Plassat JL, Hen R. A family of Drosophila serotonin
1323 receptors with distinct intracellular signalling properties and expression patterns. The EMBO
1324 journal. 1992;11(1):7-17. PubMed PMID: 1310937; PubMed Central PMCID: PMC556419.
1325 66. Witz P, Amlaiky N, Plassat JL, Maroteaux L, Borrelli E, Hen R. Cloning and
1326 characterization of a Drosophila serotonin receptor that activates adenylate cyclase.
1327 Proceedings of the National Academy of Sciences of the United States of America.
1328 1990;87(22):8940-4. PubMed PMID: 2174167; PubMed Central PMCID: PMC55076.
1329 67. Blenau W, Daniel S, Balfanz S, Thamm M, Baumann A. Dm5-HT2B: Pharmacological
1330 Characterization of the Fifth Serotonin Receptor Subtype of Drosophila melanogaster. Front
1331 Syst Neurosci. 2017;11:28. Epub 2017/05/11. doi: 10.3389/fnsys.2017.00028. PubMed PMID:
1332 28553207; PubMed Central PMCID: PMCPMC5425475.
1333 68. Gnerer JP, Venken KJ, Dierick HA. Gene-specific cell labeling using MiMIC transposons.
1334 Nucleic acids research. 2015;43(8):e56. doi: 10.1093/nar/gkv113. PubMed PMID: 25712101;
1335 PubMed Central PMCID: PMC4417149.
1336 69. Venken KJ, Schulze KL, Haelterman NA, Pan H, He Y, Evans-Holm M, et al. MiMIC: a
1337 highly versatile transposon insertion resource for engineering Drosophila melanogaster genes.
1338 Nature methods. 2011;8(9):737-43. PubMed PMID: 21985007; PubMed Central PMCID:
1339 PMC3191940.
1340 70. Diao F, Ironfield H, Luan H, Shropshire WC, Ewer J, Marr E, et al. Plug-and-play genetic
1341 access to drosophila cell types using exchangeable exon cassettes. Cell Rep. 2015;10(8):1410-
1342 21. Epub 2015/02/26. doi: 10.1016/j.celrep.2015.01.059. PubMed PMID: 25732830; PubMed
1343 Central PMCID: PMCPMC4373654.
1344 71. Fischbach KF, Dittrich APM. The optic lobe of Drosophila melanogaster. I. A
1345 Golgi analysis of wild type structure. Cell Tissue Res. 1989;258:441-75.
1346 72. Sanes JR, Zipursky SL. Design principles of insect and vertebrate visual systems.
1347 Neuron. 2010;66(1):15-36. doi: 10.1016/j.neuron.2010.01.018. PubMed PMID: 20399726;
1348 PubMed Central PMCID: PMC2871012.
1349 73. Nern A, Pfeiffer BD, Rubin GM. Optimized tools for multicolor stochastic labeling reveal
1350 diverse stereotyped cell arrangements in the fly visual system. Proceedings of the National

1351 Academy of Sciences of the United States of America. 2015;112(22):E2967-76. doi:
1352 10.1073/pnas.1506763112. PubMed PMID: 25964354; PubMed Central PMCID: PMC4460454.
1353 74. Edwards TN, Meinertzhagen IA. The functional organisation of glia in the adult brain of
1354 Drosophila and other insects. Progress in neurobiology. 2010;90(4):471-97. doi:
1355 10.1016/j.pneurobio.2010.01.001. PubMed PMID: 20109517; PubMed Central PMCID:
1356 PMC2847375.
1357 75. DeSalvo MK, Hindle SJ, Rusan ZM, Orng S, Eddison M, Halliwill K, et al. The Drosophila
1358 surface glia transcriptome: evolutionary conserved blood-brain barrier processes. Front
1359 Neurosci. 2014;8:346. Epub 2014/11/27. doi: 10.3389/fnins.2014.00346. PubMed PMID:
1360 25426014; PubMed Central PMCID: PMCPMC4224204.
1361 76. Nässel DR. Serotonin and serotonin-immunoreactive neurons in the nervous system of
1362 insects. Progress in neurobiology. 1988;30(1):1-85. PubMed PMID: 3275407.
1363 77. Xu L, He J, Kaiser A, Graber N, Schlager L, Ritze Y, et al. A Single Pair of Serotonergic
1364 Neurons Counteracts Serotonergic Inhibition of Ethanol Attraction in Drosophila. PloS one.
1365 2016;11(12):e0167518. doi: 10.1371/journal.pone.0167518. PubMed PMID: 27936023; PubMed
1366 Central PMCID: PMC5147910.
1367 78. Pooryasin A, Fiala A. Identified Serotonin-Releasing Neurons Induce Behavioral
1368 Quiescence and Suppress Mating in Drosophila. The Journal of neuroscience : the official
1369 journal of the Society for Neuroscience. 2015;35(37):12792-812. doi:
1370 10.1523/JNEUROSCI.1638-15.2015. PubMed PMID: 26377467.
1371 79. Sitaraman D, Zars M, Laferriere H, Chen YC, Sable-Smith A, Kitamoto T, et al.
1372 Serotonin is necessary for place memory in Drosophila. Proceedings of the National Academy
1373 of Sciences of the United States of America. 2008;105(14):5579-84. doi:
1374 10.1073/pnas.0710168105. PubMed PMID: 18385379; PubMed Central PMCID: PMC2291120.
1375 80. Yuan Q, Lin F, Zheng X, Sehgal A. Serotonin modulates circadian entrainment in
1376 Drosophila. Neuron. 2005;47(1):115-27. doi: 10.1016/j.neuron.2005.05.027. PubMed PMID:
1377 15996552.
1378 81. Alekseyenko OV, Chan YB, Okaty BW, Chang Y, Dymecki SM, Kravitz EA. Serotonergic
1379 Modulation of Aggression in Drosophila Involves GABAergic and Cholinergic Opposing
1380 Pathways. Current biology : CB. 2019;29(13):2145-56 e5. Epub 2019/06/25. doi:
1381 10.1016/j.cub.2019.05.070. PubMed PMID: 31231050; PubMed Central PMCID:
1382 PMCPMC6633915.
1383 82. Tuthill JC, Nern A, Holtz SL, Rubin GM, Reiser MB. Contributions of the 12 neuron
1384 classes in the fly lamina to motion vision. Neuron. 2013;79(1):128-40. doi:
1385 10.1016/j.neuron.2013.05.024. PubMed PMID: 23849200; PubMed Central PMCID:
1386 PMC3806040.
1387 83. Schmittgen TD, Livak KJ. Analyzing real-time PCR data by the comparative C(T)
1388 method. Nature protocols. 2008;3(6):1101-8. PubMed PMID: 18546601.
1389 84. Deng B, Li Q, Liu X, Cao Y, Li B, Qian Y, et al. Chemoconnectomics: Mapping Chemical
1390 Transmission in Drosophila. Neuron. 2019;101(5):876-93 e4. doi:
1391 10.1016/j.neuron.2019.01.045. PubMed PMID: 30799021.
1392 85. Qian Y, Cao Y, Deng B, Yang G, Li J, Xu R, et al. Sleep homeostasis regulated by
1393 5HT2b receptor in a small subset of neurons in the dorsal fan-shaped body of drosophila. Elife.
1394 2017;6. doi: 10.7554/eLife.26519. PubMed PMID: 28984573; PubMed Central PMCID:
1395 PMC5648528.
1396 86. Macpherson LJ, Zaharieva EE, Kearney PJ, Alpert MH, Lin TY, Turan Z, et al. Dynamic
1397 labelling of neural connections in multiple colours by trans-synaptic fluorescence
1398 complementation. Nat Commun. 2015;6:10024. Epub 2015/12/04. doi: 10.1038/ncomms10024.
1399 PubMed PMID: 26635273; PubMed Central PMCID: PMCPMC4686661.
1400 87. Trueta C, De-Miguel FF. Extrasynaptic exocytosis and its mechanisms: a source of
1401 molecules mediating volume transmission in the nervous system. Frontiers in physiology.

2012;3:319. doi: 10.3389/fphys.2012.00319. PubMed PMID: 22969726; PubMed Central PMCID: PMC3432928.
88. Bunin MA, Wightman RM. Paracrine neurotransmission in the CNS: involvement of 5-HT. Trends Neurosci. 1999;22(9):377-82. PubMed PMID: 10441294.
89. Vizi ES, Fekete A, Karoly R, Mike A. Non-synaptic receptors and transporters involved in brain functions and targets of drug treatment. British journal of pharmacology. 2010;160(4):785-809. doi: 10.1111/j.1476-5381.2009.00624.x. PubMed PMID: 20136842; PubMed Central PMCID: PMC2935987.
90. Fuxe K, Dahlstrom AB, Jonsson G, Marcellino D, Guescini M, Dam M, et al. The discovery of central monoamine neurons gave volume transmission to the wired brain. Progress in neurobiology. 2010;90(2):82-100. doi: 10.1016/j.pneurobio.2009.10.012. PubMed PMID: 19853007.
91. Hoyer D, Hannon JP, Martin GR. Molecular, pharmacological and functional diversity of 5-HT receptors. Pharmacol Biochem Behav. 2002;71(4):533-54. PubMed PMID: 11888546.
92. Chen TW, Wardill TJ, Sun Y, Pulver SR, Renninger SL, Baohan A, et al. Ultrasensitive fluorescent proteins for imaging neuronal activity. Nature. 2013;499(7458):295-300. doi: 10.1038/nature12354. PubMed PMID: 23868258; PubMed Central PMCID: PMC3777791.
93. Liu C, Meng Z, Wiggin TD, Yu J, Reed ML, Guo F, et al. A Serotonin-Modulated Circuit Controls Sleep Architecture to Regulate Cognitive Function Independent of Total Sleep in Drosophila. Current biology : CB. 2019;29(21):3635-46 e5. Epub 2019/11/02. doi: 10.1016/j.cub.2019.08.079. PubMed PMID: 31668619; PubMed Central PMCID: PMCPMC6832866.
94. Narahashi T. Tetrodotoxin: a brief history. Proc Jpn Acad Ser B Phys Biol Sci. 2008;84(5):147-54. Epub 2008/10/23. doi: 10.2183/pjab.84.147. PubMed PMID: 18941294; PubMed Central PMCID: PMCPMC2858367.
95. Narahashi T, Moore JW, Scott WR. Tetrodotoxin Blockage of Sodium Conductance Increase in Lobster Giant Axons. The Journal of general physiology. 1964;47:965-74. Epub 1964/05/01. doi: 10.1085/jgp.47.5.965. PubMed PMID: 14155438; PubMed Central PMCID: PMCPMC2195365.
96. Mu L, Ito K, Bacon JP, Strausfeld NJ. Optic glomeruli and their inputs in Drosophila share an organizational ground pattern with the antennal lobes. The Journal of neuroscience : the official journal of the Society for Neuroscience. 2012;32(18):6061-71. doi: 10.1523/JNEUROSCI.0221-12.2012. PubMed PMID: 22553013; PubMed Central PMCID: PMC3358351.
97. Juusola M, Uusitalo RO, Weckstrom M. Transfer of graded potentials at the photoreceptor-interneuron synapse. The Journal of general physiology. 1995;105(1):117-48. doi: 10.1085/jgp.105.1.117. PubMed PMID: 7537323; PubMed Central PMCID: PMC2216927.
98. Uusitalo RO, Juusola M, Kouvalainen E, Weckstrom M. Tonic transmitter release in a graded potential synapse. Journal of neurophysiology. 1995;74(1):470-3. doi: 10.1152/jn.1995.74.1.470. PubMed PMID: 7472349.
99. Polter AM, Li X. 5-HT1A receptor-regulated signal transduction pathways in brain. Cell Signal. 2010;22(10):1406-12. Epub 2010/04/02. doi: 10.1016/j.cellsig.2010.03.019. PubMed PMID: 20363322; PubMed Central PMCID: PMCPMC2903656.
100. Cao G, Platisa J, Pieribone VA, Raccuglia D, Kunst M, Nitabach MN. Genetically targeted optical electrophysiology in intact neural circuits. Cell. 2013;154(4):904-13. Epub 2013/08/08. doi: 10.1016/j.cell.2013.07.027. PubMed PMID: 23932121; PubMed Central PMCID: PMCPMC3874294.
101. Maisak MS, Haag J, Ammer G, Serbe E, Meier M, Leonhardt A, et al. A directional tuning map of Drosophila elementary motion detectors. Nature. 2013;500(7461):212-6. doi: 10.1038/nature12320. PubMed PMID: 23925246.

1452 102. Takemura SY, Nern A, Chklovskii DB, Scheffer LK, Rubin GM, Meinertzhagen IA. The
1453 comprehensive connectome of a neural substrate for 'ON' motion detection in Drosophila. Elife.
1454 2017;6. doi: 10.7554/eLife.24394. PubMed PMID: 28432786; PubMed Central PMCID:
1455 PMC5435463.
1456 103. Stuart AE, Borycz J, Meinertzhagen IA. The dynamics of signaling at the histaminergic
1457 photoreceptor synapse of arthropods. Progress in neurobiology. 2007;82(4):202-27. doi:
1458 10.1016/j.pneurobio.2007.03.006. PubMed PMID: 17531368.
1459 104. Chaturvedi R, Reddig K, Li HS. Long-distance mechanism of neurotransmitter recycling
1460 mediated by glial network facilitates visual function in Drosophila. Proceedings of the National
1461 Academy of Sciences of the United States of America. 2014;111(7):2812-7. doi:
1462 10.1073/pnas.1323714111. PubMed PMID: 24550312; PubMed Central PMCID: PMC3932938.
1463 105. Nikolaev A, Zheng L, Wardill TJ, O'Kane CJ, de Polavieja GG, Juusola M. Network
1464 adaptation improves temporal representation of naturalistic stimuli in Drosophila eye: II
1465 mechanisms. PloS one. 2009;4(1):e4306. doi: 10.1371/journal.pone.0004306. PubMed PMID:
1466 19180195; PubMed Central PMCID: PMC2628722.
1467 106. Fisher YE, Yang HH, Isaacman-Beck J, Xie M, Gohl DM, Clandinin TR. FlpStop, a tool
1468 for conditional gene control in Drosophila. eLife. 2017;6. Epub 2017/02/18. doi:
1469 10.7554/eLife.22279. PubMed PMID: 28211790; PubMed Central PMCID: PMCPMC5342825.
1470 107. Kolodziejczyk A, Sun X, Meinertzhagen IA, Nassel DR. Glutamate, GABA and
1471 acetylcholine signaling components in the lamina of the Drosophila visual system. PloS one.
1472 2008;3(5):e2110. doi: 10.1371/journal.pone.0002110. PubMed PMID: 18464935; PubMed
1473 Central PMCID: PMC2373871.
1474 108. Chang H-Y, Grygoruk A, Brooks ES, Ackerson LC, Maidment NT, Bainton RJ, et al.
1475 Over-expression of the Drosophila vesicular monoamine transporter increases motor activity
1476 and courtship but decreases the behavioral response to cocaine. Molecular Psychiatry.
1477 2006;11:99-113.
1478 109. Monastirioti M. Biogenic amine systems in the fruit fly Drosophila melanogaster.
1479 Microscopy research and technique. 1999;45(2):106-21. doi: 10.1002/(SICI)1097-
1480 0029(19990415)45:2<106::AID-JEMT5>3.0.CO;2-3. PubMed PMID: 10332728.
1481 110. Descarries L, Mechawar N. Ultrastructural evidence for diffuse transmission by
1482 monoamine and acetylcholine neurons of the central nervous system. Prog Brain Res.
1483 2000;125:27-47. doi: 10.1016/S0079-6123(00)25005-X. PubMed PMID: 11098652.
1484 111. Coates KE, Majot AT, Zhang X, Michael CT, Spitzer SL, Gaudry Q, et al. Identified
1485 Serotonergic Modulatory Neurons Have Heterogeneous Synaptic Connectivity within the
1486 Olfactory System of Drosophila. The Journal of neuroscience : the official journal of the Society
1487 for Neuroscience. 2017;37(31):7318-31. doi: 10.1523/JNEUROSCI.0192-17.2017. PubMed
1488 PMID: 28659283; PubMed Central PMCID: PMC5546105.
1489 112. Gaspar P, Lillesaar C. Probing the diversity of serotonin neurons. Philosophical
1490 transactions of the Royal Society of London Series B, Biological sciences.
1491 2012;367(1601):2382-94. doi: 10.1098/rstb.2011.0378. PubMed PMID: 22826339; PubMed
1492 Central PMCID: PMC3405676.
1493 113. Herve D, Pickel VM, Joh TH, Beaudet A. Serotonin axon terminals in the ventral
1494 tegmental area of the rat: fine structure and synaptic input to dopaminergic neurons. Brain Res.
1495 1987;435(1-2):71-83. PubMed PMID: 2892580.
1496 114. Moukhles H, Bosler O, Bolam JP, Vallee A, Umbriaco D, Geffard M, et al. Quantitative
1497 and morphometric data indicate precise cellular interactions between serotonin terminals and
1498 postsynaptic targets in rat substantia nigra. Neuroscience. 1997;76(4):1159-71. PubMed PMID:
1499 9027876.
1500 115. Nässel DR, Elekes K. Ultrastructural demonstration of serotonin-immunoreactivity in the
1501 nervous system of an insect (Calliphora erythrocephala). Neurosci Lett. 1984;48(2):203-10.
1502 PubMed PMID: 6384830.

1503 116. Marder E. Variability, compensation, and modulation in neurons and circuits.
1504 Proceedings of the National Academy of Sciences of the United States of America. 2011;108
1505 Suppl 3:15542-8. doi: 10.1073/pnas.1010674108. PubMed PMID: 21383190; PubMed Central
1506 PMCID: PMC3176600.
1507 117. Prinz AA, Thirumalai V, Marder E. The functional consequences of changes in the
1508 strength and duration of synaptic inputs to oscillatory neurons. The Journal of neuroscience :
1509 the official journal of the Society for Neuroscience. 2003;23(3):943-54. PubMed PMID:
1510 12574423; PubMed Central PMCID: PMC6741924.
1511 118. Takemura SY, Karuppudurai T, Ting CY, Lu Z, Lee CH, Meinertzhagen IA. Cholinergic
1512 circuits integrate neighboring visual signals in a Drosophila motion detection pathway. Current
1513 biology : CB. 2011;21(24):2077-84. Epub 2011/12/01. doi: 10.1016/j.cub.2011.10.053. PubMed
1514 PMID: 22137471; PubMed Central PMCID: PMCPMC3265035.
1515 119. Shinomiya K, Karuppudurai T, Lin TY, Lu Z, Lee CH, Meinertzhagen IA. Candidate
1516 neural substrates for off-edge motion detection in Drosophila. Current biology : CB.
1517 2014;24(10):1062-70. Epub 2014/04/24. doi: 10.1016/j.cub.2014.03.051. PubMed PMID:
1518 24768048; PubMed Central PMCID: PMCPMC4031294.
1519 120. Halberstadt AL. Recent advances in the neuropsychopharmacology of serotonergic
1520 hallucinogens. Behav Brain Res. 2015;277:99-120. Epub 2014/07/15. doi:
1521 10.1016/j.bbr.2014.07.016. PubMed PMID: 25036425; PubMed Central PMCID:
1522 PMCPMC4642895.
1523 121. Li YH, Xiang K, Xu X, Zhao X, Li Y, Zheng L, et al. Co-activation of both 5-HT1A and 5-
1524 HT7 receptors induced attenuation of glutamatergic synaptic transmission in the rat visual
1525 cortex. Neurosci Lett. 2018;686:122-6. Epub 2018/09/08. doi: 10.1016/j.neulet.2018.09.013.
1526 PubMed PMID: 30205142.
1527 122. Sizemore TR, Dacks AM. Serotonergic Modulation Differentially Targets Distinct
1528 Network Elements within the Antennal Lobe of Drosophila melanogaster. Scientific reports.
1529 2016;6:37119. doi: 10.1038/srep37119. PubMed PMID: 27845422; PubMed Central PMCID:
1530 PMC5109230.
1531 123. Gordon MD, Scott K. Motor control in a Drosophila taste circuit. Neuron. 2009;61(3):373-
1532 84. doi: 10.1016/j.neuron.2008.12.033. PubMed PMID: 19217375; PubMed Central PMCID:
1533 PMC2650400.
1534 124. Boppana S, Kendall N, Akinrinsola O, White D, Patel K, Lawal H. Immunolocalization of
1535 the vesicular acetylcholine transporter in larval and adult Drosophila neurons. Neurosci Lett.
1536 2017;643:76-83. Epub 2017/02/07. doi: 10.1016/j.neulet.2017.02.012. PubMed PMID:
1537 28188850; PubMed Central PMCID: PMCPMC5382984.
1538 125. Schindelin J, Arganda-Carreras I, Frise E, Kaynig V, Longair M, Pietzsch T, et al. Fiji: an
1539 open-source platform for biological-image analysis. Nature methods. 2012;9(7):676-82. Epub
1540 2012/06/28. doi: 10.1038/nmeth.2019. PubMed PMID: 22743772; PubMed Central PMCID:
1541 PMCPMC3855844.
1542 126. Tan L, Zhang KX, Pecot MY, Nagarkar-Jaiswal S, Lee PT, Takemura SY, et al. Ig
1543 Superfamily Ligand and Receptor Pairs Expressed in Synaptic Partners in Drosophila. Cell.
1544 2015;163(7):1756-69. doi: 10.1016/j.cell.2015.11.021. PubMed PMID: 26687360; PubMed
1545 Central PMCID: PMC4804707.
1546 127. Hu Y, Sopko R, Foos M, Kelley C, Flockhart I, Ammeux N, et al. FlyPrimerBank: an
1547 online database for Drosophila melanogaster gene expression analysis and knockdown
1548 evaluation of RNAi reagents. G3 (Bethesda). 2013;3(9):1607-16. Epub 2013/09/04. doi:
1549 10.1534/g3.113.007021. PubMed PMID: 23893746; PubMed Central PMCID:
1550 PMCPMC3755921.
1551 128. Picelli S, Bjorklund AK, Faridani OR, Sagasser S, Winberg G, Sandberg R. Smart-seq2
1552 for sensitive full-length transcriptome profiling in single cells. Nature methods.
1553 2013;10(11):1096-8. doi: 10.1038/nmeth.2639. PubMed PMID: 24056875.

1554 129. Picelli S, Faridani OR, Bjorklund AK, Winberg G, Sagasser S, Sandberg R. Full-length
1555 RNA-seq from single cells using Smart-seq2. Nature protocols. 2014;9(1):171-81. doi:
1556 10.1038/nprot.2014.006. PubMed PMID: 24385147.
1557 130. Dobin A, Davis CA, Schlesinger F, Drenkow J, Zaleski C, Jha S, et al. STAR: ultrafast
1558 universal RNA-seq aligner. Bioinformatics. 2013;29(1):15-21. doi:
1559 10.1093/bioinformatics/bts635. PubMed PMID: 23104886; PubMed Central PMCID:
1560 PMC3530905.
1561 131. Keles MF, Frye MA. Object-Detecting Neurons in Drosophila. Current biology : CB.
1562 2017;27(5):680-7. doi: 10.1016/j.cub.2017.01.012. PubMed PMID: 28190726; PubMed Central
1563 PMCID: PMCPMC5340600.
1564 132. Weir PT, Dickinson MH. Functional divisions for visual processing in the central brain of
1565 flying Drosophila. Proceedings of the National Academy of Sciences of the United States of
1566 America. 2015;112(40):E5523-32. Epub 2015/09/02. doi: 10.1073/pnas.1514415112. PubMed
1567 PMID: 26324910; PubMed Central PMCID: PMCPMC4603480.
1568 133. Wilson RI, Turner GC, Laurent G. Transformation of olfactory representations in the
1569 Drosophila antennal lobe. Science. 2004;303(5656):366-70. Epub 2003/12/18. doi:
1570 10.1126/science.1090782. PubMed PMID: 14684826.
1571 134. Akin O, Zipursky SL. Frazzled promotes growth cone attachment at the source of a
1572 Netrin gradient in the Drosophila visual system. Elife. 2016;5. doi: 10.7554/eLife.20762.
1573 PubMed PMID: 27743477; PubMed Central PMCID: PMC5108592.

1574

1575

1576